Stability of Constrained Capillary Surfaces

J.B. Bostwick[1] and P.H. Steen[2]

[1]Department of Engineering Science and Applied Mathematics, Northwestern University, Evanston, Illinois 60208

[2]School of Chemical and Biomolecular Engineering and Center for Applied Mathematics, Cornell University, Ithaca, New York 14853; email: PHS7@cornell.edu

Annu. Rev. Fluid Mech. 2015. 47:539–68

First published online as a Review in Advance on September 29, 2014

The *Annual Review of Fluid Mechanics* is online at fluid.annualreviews.org

This article's doi:
10.1146/annurev-fluid-010814-013626

Keywords

surface tension, wetting, drops, bridges, rivulets, contact line, common line

Abstract

A capillary surface is an interface between two fluids whose shape is determined primarily by surface tension. Sessile drops, liquid bridges, rivulets, and liquid drops on fibers are all examples of capillary shapes influenced by contact with a solid. Capillary shapes can reconfigure spontaneously or exhibit natural oscillations, reflecting static or dynamic instabilities, respectively. Both instabilities are related, and a review of static stability precedes the dynamic case. The focus of the dynamic case here is the hydrodynamic stability of capillary surfaces subject to constraints of (*a*) volume conservation, (*b*) contact-line boundary conditions, and (*c*) the geometry of the supporting surface.

1. OVERVIEW

Capillary surface: a mathematical surface between two fluids endowed with surface tension

Volume (pressure) disturbance: disturbance that preserves the volume (pressure) of the base state

Plateau-Rayleigh (PR) limit: the length, equal to its base-state circumference, beyond which a cylindrical capillary surface is unstable to volume disturbances

Plateau tank: a chamber that enables large l_c on Earth by immersing a capillary surface in an immiscible liquid of nearly the same density

Sessile drop: a liquid drop on a solid substrate

Liquid bridge: a liquid enclosed by a capillary surface having two closed-curve contact lines located on separate solid surfaces

Capillary surfaces are at once a modern and classical topic. Shape reconfiguration is central to emerging applications that exploit the physics of liquids confined by surface tension on the micro- and nanoscale, whereas the study of shape stability reaches back to the 1800s (see the sidebar Historical Perspective). We review recent progress in the dynamic stability analysis of surfaces, focusing on the influence of constraint by solid supports.

An early stability prediction is due to Plateau (1863), who reported the instability to volume disturbances of a capillary cylinder for lengths longer than its circumference, the well-known Plateau limit. Some years later, Rayleigh (1879) calculated the growth rate of instability as it depends on the disturbance wave number to estimate the final droplet size for a liquid jet disintegrating into droplets. The Plateau limit is recovered from Rayleigh's solution of the hydrodynamic problem by putting the growth rate to zero [the Plateau limit is sometimes referred to as the Plateau-Rayleigh (PR) limit]. This illustrates how static stability can be recovered from a dynamic analysis and provides the prototypical relationship between the stabilities, a theme of this review.

Surface tension largely determines the surface shape on scales smaller than the capillary length $l_c \equiv (\sigma/\rho g)^{1/2}$, where ρg is the buoyant force per volume according to the gravity level g and the density difference between the fluids ρ. For fluids separated by a thin film (e.g., soap films) or a fluid against an immiscible fluid (e.g., Plateau tanks), the density difference ρ can be small, yielding tens-of-centimeter capillary lengths. In space applications, the capillary length for a liquid against gas can be 100 cm, whereas it is usually a few millimeters on Earth.

Michael (1981) gave a then-timely snapshot of the field in this journal, with an emphasis on static stability and methods. Interest in shape stability, with its enhanced role in low-gravity fluid mechanics, grew as space programs grew. Myshkis et al. (1987) provided a comprehensive monograph with this motivation. Also informed by capillarity in weightlessness is Langbein (2002). De Gennes (1985) paid particular attention to wetting and spreading, which culminated in a comprehensive account of capillary phenomena (de Gennes et al. 2010). Rowlinson & Widom (2002) and others in the chemistry community provided a molecular perspective, and yet another thread, with mathematical roots in the study of isoperimetric inequalities, has been provided by Finn (1999). Johns & Narayanan (2002) presented case studies in capillary stability, whereas Shikhmurzaev (2007) focused more on the flows that underlie capillary surfaces. In this article, we focus on the mechanics of fluids subject to capillary instability.

Between 1994 and 2013, items published annually that list the terms sessile drop, liquid bridge, or liquid rivulet as a topic have surged nearly sixfold in number (**Figure 1*a***). Nearly 3,000 publications have appeared in total. Using the terms capillarity, wetting, or spreading as alternative

HISTORICAL PERSPECTIVE

Popular public lectures by Boys in the 1890s featured soap-film experiments. Boys (1959 [1890]) attributed these experiments in capillarity to the published work of Savart, Plateau, Maxwell, Thomson, Rayleigh, Bell, and Rücker. An entry on capillary action first appeared in the *Encyclopedia Britannica* in 1898 (Maxwell 1898), reflecting the mathematical physicists' wide interest in the subject at that time (e.g., Schrödinger 1915). About one-third of the 14-page entry speaks to the stability of capillary surfaces. The entry remains in the encyclopedia until 1926, at which time it redirects readers to an entry on surface tension, with an indication that Lord Rayleigh has taken over authorship, at least for the historical review part. Regarding the 1898 entry, Erle et al. (1970) pointed out that Maxwell confused volume and pressure disturbances in his discussion of the stability of the catenoid.

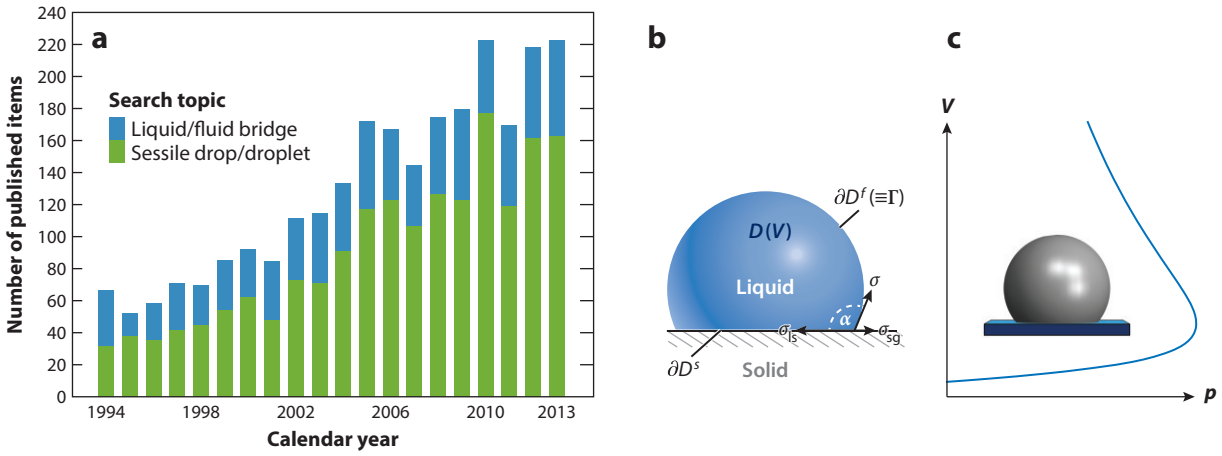

Figure 1

(*a*) Number of publications by year since 1994 found by searching on listed topics. (*b*) Definition sketch for a sessile drop of volume V and equilibrium contact-angle α, with liquid/gas (σ), liquid/solid (σ_{ls}), and solid/gas (σ_{sg}) interfacial energies per area. (*c*) Sessile drop response diagram for a pinned contact line: volume V against Laplace pressure p.

topics shows an even stronger swell. Feeding this are streams of interest from new applications, mainly on the micro- and nanoscales. For droplets, these applications include nanoparticle assembly by droplet evaporation (Bigioni et al. 2006), the assembly of microparts via capillarity (Sariola et al. 2010), microassays for screening (Berthier et al. 2008), microencapsulation (Almeida et al. 2008), forensic bloodstains (Attinger et al. 2013), immersion lithography at high speeds (Harder et al. 2008), the cleaning of nanopatterned wafers (Xu et al. 2013, Shahraz et al. 2012), biomimetic surface design (Lafuma & Quéré 2003, Tuteja et al. 2007), and surface wettability engineering generally. Contact-angle measurement continues to be a principal means for the assessment of material wettability in many industries (Matsumoto & Nogi 2008, Seetharaman et al. 2013). For liquid bridges, applications include gravure printing (Dodds et al. 2012, Kumar 2015), colloidal aggregation (Kralchevsky & Denkov 2001), solid adhesion (Maugis 2000), bioinspired adhesion (De Souza et al. 2008, Slater et al. 2012, van Lengerich & Steen 2012), crystal growth in float zones (Lappa 2005), and extensional rheology (McKinley & Sridhar 2002), whereas, for rivulets, they include heat and mass transfer (El-Genk & Saber 2001). Inexpensive access to high-speed imaging cameras may also be playing a role in the swell of interest.

Simulations (Sui et al. 2014) and experiments (Milne et al. 2014) are crucial to the subject's development. Related, but also outside the scope of the present review, are thin films and coating flows (Oron et al. 1997); Marangoni flows (Matar & Craster 2009); the nonlinear dynamics of topological change that sometimes ensues from capillary instability (Eggers 1997, Paulsen et al. 2012); and software such as Surface Evolver (Brakke 1992), a versatile tool for predicting the reconfiguration of static surfaces (Collicott & Weislogel 2004).

Liquids that partially wet a solid support are of interest (**Figure 1*b***). For these, liquid-gas (A_{lg}), liquid-solid (A_{ls}), and solid-gas (A_{sg}) surface areas can all change upon shape reconfiguration. The free energy U of a configuration is given by the sum of its surface areas A weighted by the corresponding interfacial energies per area (equivalently, surface tensions) σ,

$$U = \sigma A_{lg} + \sigma_{ls} A_{ls} + \sigma_{sg} A_{sg}. \quad (1)$$

Contact angle: angle measured through a liquid, from the solid to the capillary surface; a static or equilibrium contact angle relates the liquid/gas, liquid/solid, and solid/gas surface energies through the Young-Dupré equation

Rivulet: a liquid stream on a solid substrate

Dry solid appears at the same rate that liquid recedes, $\delta A_{sg} = -\delta A_{ls}$, enabling a reduced energy functional to be defined,

$$\mathcal{A} \equiv A_{lg} - \mathcal{M} A_{ls}, \tag{2}$$

where $\mathcal{M} \equiv (\sigma_{sg} - \sigma_{ls})/\sigma$ is the relative affinity of the partially wetting liquid for the solid, with $-1 \leq \mathcal{M} \leq 1$. If material properties are such that $\mathcal{M}$ falls outside $(-1, 1)$, the liquid completely wets ($\mathcal{M} > 1$) or dewets ($\mathcal{M} < -1$) the solid.

Contact line (CL): the line intersection of a capillary surface with a solid support surface; common to liquid, gas, and solid phases

Fold: a turning point

Response diagram: a plot of force-like response against deflection-like displacement, as in a pressure-volume diagram

Stability determinations are sensitive to the class of allowable disturbances. Perhaps the greatest sensitivity is to fixed (pinned) or moving (free) contact lines (CLs), as these control whether one or two competitors are active in the competition to decrease $\mathcal{A}$. For pinned CLs ($\delta A_{ls} = 0$), only the liquid-gas area can change, $\delta\mathcal{A} = \delta A_{lg}$, whereas for free CLs, both δA_{lg} and δA_{ls} can be of either sign. The overall competition, determined for equilibrium by $\delta\mathcal{A} = 0$ and for stability (sufficient) by $\delta^2\mathcal{A} > 0$, depends on the weight $\mathcal{M}$, which can have either sign, depending on whether the liquid is wetting, $\cos\alpha > 0$, or nonwetting, $\cos\alpha < 0$, as the equilibrium contact angle α is related, $\cos\alpha = \mathcal{M}$ (Section 2.2).

Stability is also sensitive to constraints on the bulk—whether pressure or volume disturbances are allowed. Let us consider a surface area A_{lg} enclosing a liquid volume V so that A_{lg} depends on V alone, as for the sessile drop in **Figure 1*c***with V controlled by injection through the base, for example. For a large class of shapes, including those of constant mean curvature with pinned CL, it has been shown that

$$\frac{dA_{lg}}{dV} = \frac{p}{\sigma}, \tag{3}$$

where $p(V)$ is the capillary pressure difference across the surface (Gauss 1830, Gillette & Dyson 1974). According to Equation 3, equilibrium ($dA_{lg}/dV = 0$) requires $p = 0$, and for stability ($d^2A_{lg}/dV^2 > 0$), $dp/dV > 0$. We note that this calculation does not account for any constraint on the disturbance volume.

The criterion for stability, $dp/dV > 0$, turns out to be sufficient but not necessary. A thought experiment illustrates (see **Figure 1*c***). For a disturbance at constant pressure (referred to as a pressure disturbance) that adds volume, when $dp/dV > 0$, the drop in equilibrium responds with greater pressure, expelling the newly added volume and falling back to equilibrium. This is stability. When $dp/dV < 0$, the opposite occurs, giving instability. That is, below (above) the fold in the pV curve, the sessile drop is stable (unstable). Alternatively, for a disturbance that preserves the volume, a volume disturbance, the entire family of equilibria is stable. In summary, below the fold, the equilibria are stable to both disturbances, whereas, above the fold, they are stable to volume but not to pressure disturbances. To obtain this stability result by calculus of the second variation from Equations 2 and 3, one must account for the volume constraint. Poincaré (1885) provided an approach that circumvents calculation of the second variation, $\delta^2\mathcal{A}$, giving both pressure and volume stability changes from folds in the response diagram, which consists of a family of equilibria (see Section 2.4).

Reconfiguration by surface tension occurs dynamically at speeds $u \equiv (\sigma/\rho\ell)^{1/2}$, which can be used to define an inverse Reynolds number, the Ohnesorge number, $Oh \equiv \mu/(\rho\ell\sigma)^{1/2}$, where μ is the dynamic viscosity. We note that the reconfiguration speed u increases with decreasing scale ℓ. For $\ell \sim 0.1$ mm and water in air, one obtains $Oh \sim 10^{-2}$. Basaran (2002) gave examples of inviscid behavior at scales well below 1 mm. Low–Ohnesorge number flows are our interest here.

In summary, our goal is to illustrate the mathematical theory of capillary instability using relevant examples to guide the reader to the forefront of this exciting field. The challenge is to develop a perspective that yields rules of thumb for the practitioner.

Common configurations are given in **Figure 2*d–f***. The far-left column of **Figure 2** highlights sessile supports of varying primary curvatures, whereas the far-right column highlights varying

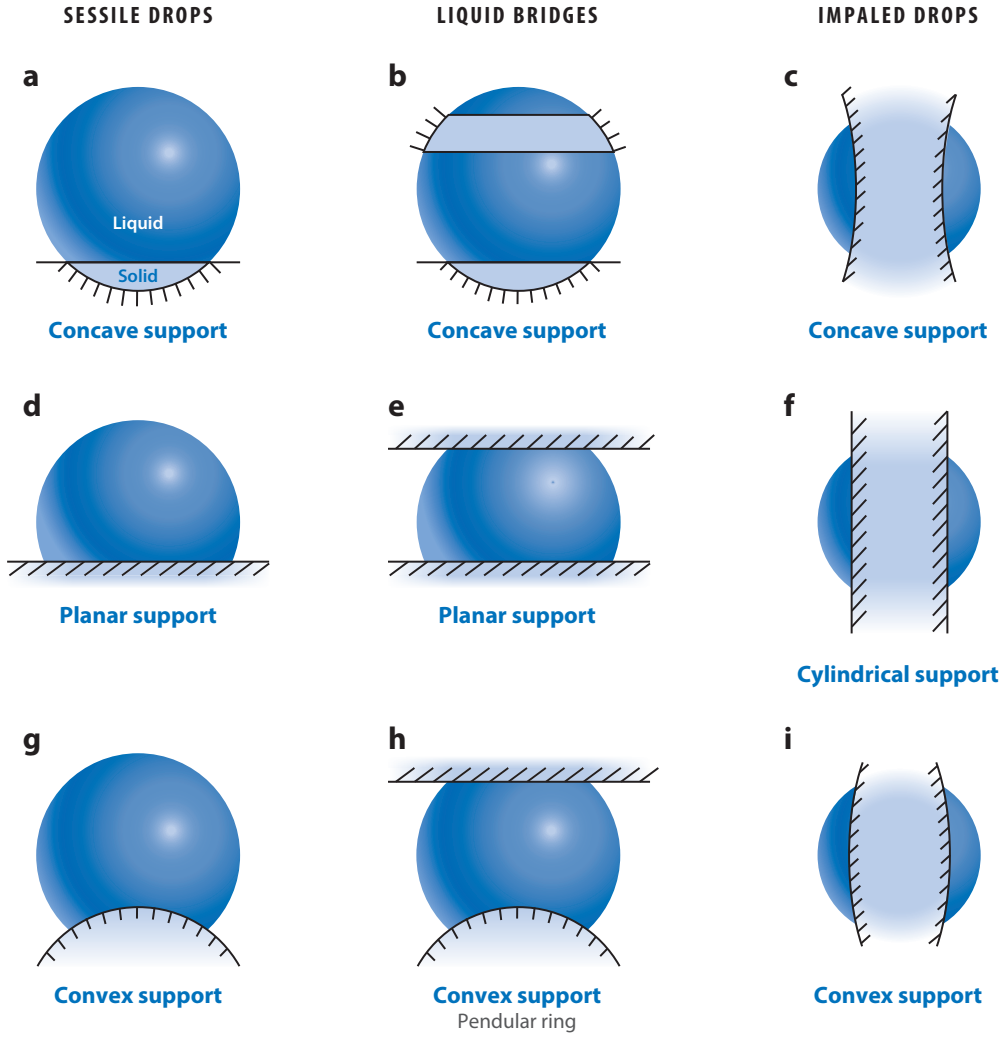

Figure 2

Spherical surface configurations with axisymmetric support geometry.

secondary curvatures. The middle column of the figure shows liquid bridge configurations. When a dome support is part of a bridge, the configuration is a pendular ring (**Figure 2*b***), and a latitudinal belt is referred to as a spherical belt (**Figure 2*b***).

The columns in **Figure 2** show families that can be related by the support variation. As such, the stability results for one family member can often be inferred from those of another. Canonical support geometries represent each column: the sessile drop, liquid bridge, and impaled drop (**Figure 2*d–f***, respectively). A sessile drop is related to a free drop and a liquid bridge to a cylindrical bridge, and both are related through a disintegrating jet, as discussed above. In addition to their organizational utility, such familial relationships, mathematically formalized through problem homotopy, can be useful for quantitative predictions (see Section 3.2.2).

Homotopy: a continuous map relating one support geometry to another and, thereby, one system of equations and boundary conditions (or problem) to another

Figure 3 illustrates influences of solid support on static stability. Helical supports enable long liquid columns. **Figure 3*a*** shows a liquid filling a stretched spring and the column near

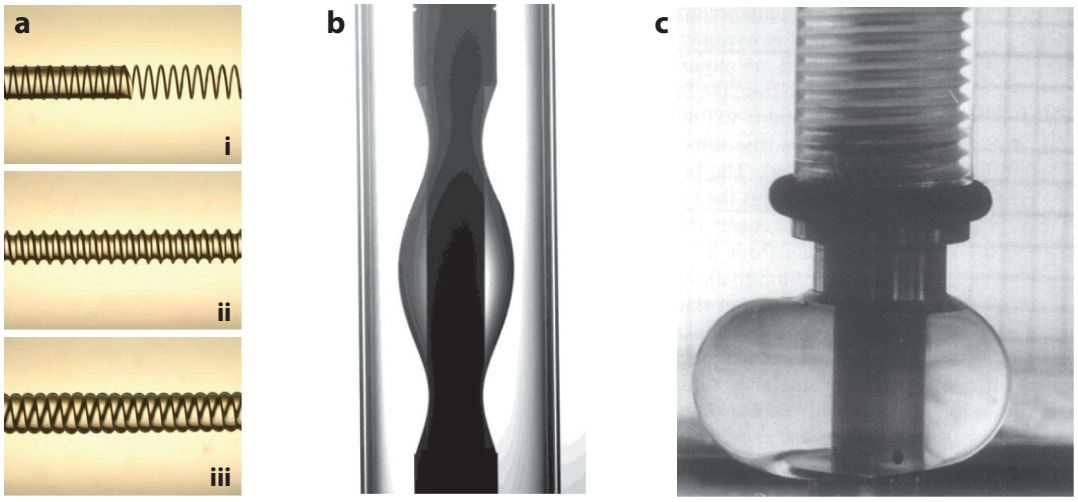

Figure 3

Photographs of static shapes in Plateau tanks. (*a*) Liquid filling a stretched spring (*i*) and the liquid column near its (*ii*) minimum-volume and (*iii*) maximum-volume stability limits. Panel *a* reproduced with permission from Lowry & Thiessen (2007). (*b*) Flow control revealing the pearl-shaped mode, the next static instability beyond the Plateau-Rayleigh limit (Lowry & Steen 1997). Photograph courtesy of Brian Lowry. (*c*) Beer-belly shape observed when an impaled drop (liquid bridge) is squeezed by end supports at a fixed volume, typical of the azimuthal instability seen when the Steiner limit is exceeded. Panel *c* reproduced with permission from Russo & Steen (1986).

its minimum-volume and maximum-volume stability limits. **Figure 3*b*** shows a flow-influenced PR instability. After an unconstrained PR instability, an amphora shape appears while here an annular external flow stabilizes the first instability mode so that the surface collapses at the second instability mode, exhibiting a pearl-shaped configuration. In **Figure 3*c***, on decreasing length at a fixed volume, the impaled drop (or liquid bridge) suffers an azimuthal instability at the Steiner limit.

Configurational equilibrium requires bulk, surface, and CL equilibrium. Bulk equilibrium requires an equilibrated hydrostatic pressure field throughout the liquid. Surface equilibrium requires the pressure at the liquid surface to match the Young-Laplace pressure. Finally, CL equilibrium requires either a fixed CL (the pinned condition) or a mobile CL with a fixed equilibrium contact angle (the free condition), as required by the Young-Dupré equation.

Provided gravity is neglected, all configurations in **Figure 2** are in bulk and surface equilibrium as each shape is a spherical section. Solid properties must be accommodating for CL equilibrium to obtain. That is, the solid supports must be arranged, via local geometry (sharp corners) or chemistry (material properties), to yield a pinned or free CL. For the pinned CL, all the capillary surfaces of **Figure 2** are statically stable. Stability is an immediate consequence of (*a*) the local minimum of the surface energy of the spherical shape and (*b*) the restriction of the class of disturbances caused by pinning the CL(s). That is, if the free sphere is stable locally (isoperimetric inequality), a section of a sphere with a pinned boundary must also be stable, as it is subject to fewer disturbances. In contrast, if the CL is free, the capillary figures may be unstable, even if they are in CL equilibrium. A free CL brings the surface energy of the solid into play, adding a degree of freedom to the competition that can be destabilizing. For example, for a thick wire, the impaled drop in the far-right column of **Figure 2** can lower the liquid-solid-gas system energy by shifting to the perimeter of the wire, breaking axisymmetry, and becoming more like an isolated drop (Quéré 1999).

Azimuthal mode or shape: mode or disturbance shape that breaks rotational symmetry

In summary, when a solid is introduced to support a drop, the free surface becomes constrained. This is stabilizing because it narrows the class of disturbances. Conversely, if the CL is free to wet or dewet the solid, a new freedom arises, which is destabilizing. The competition between the stabilizing and destabilizing effect is our subject. For dynamic stability, in addition to these complications, the solid support introduces the laboratory frame, which can introduce a low-frequency oscillation mode. We now discuss progress in resolving this competition, first for the static and then for the dynamic disturbances.

Turning point (TP): a point in the preferred diagram at which the response curve has a horizontal or vertical tangent, turning back without crossing

2. HISTORICAL FOUNDATIONS AND STATIC STABILITY

Interest in capillary phenomena began in the 1700s when Segner (1751) first postulated the concept of surface tension. Young (1805) and Laplace (1806) made the subject quantitative. Whereas Young preferred to use forces, Gauss (1830) promoted the energy-minimization approach. This required the calculus of variations. The equations governing the extremals and minimizers for supported capillary shapes have been known for more than 100 years (Bolza 1904). We record them here to establish the parallel formalism with the dynamic problem, using the notation of Myshkis et al. (1987). We then discuss alternate solution methods to the direct calculation of the second variation, such as the Poincaré turning-point (TP) method, and place them in a historical context (see the sidebar Rotating, Self-Gravitating Figures of Equilibrium). Finally, we briefly review the stability of systems of capillary elements, including capillary switches and compound drop and bridge systems.

2.1. Energy Functional

A liquid that partially wets a solid substrate has potential energy U given by Equation 1. In many situations, the volume V enclosed by the capillary surface is held constant:

$$V[\mathbf{x}] \equiv \int_V \mathrm{d}V = C \quad [D]. \tag{4}$$

ROTATING, SELF-GRAVITATING FIGURES OF EQUILIBRIUM

The shape of a rotating self-gravitating liquid body was of sustained mathematical interest for more than a century, beginning with Newton's prediction of Earth being a sphere flattened at the poles. This model of planetary evolution depends on the gravitational strength and rotational rate. Two-parameter families of equilibrium shapes and their stability were studied by Maclaurin, Jacobi, Meyer, Liouville, Dirichlet, Dedekind, and Riemann, among others. Chandrasekhar (1987) provided a historical account of their efforts, along with the many missteps that were made. As part of the discussion at the time, Poincaré (1885) showed that TPs along solution branches signal stability changes and thereby provided an economical way to track stability. For these historical reasons, the astrophysics community has probably had a greater awareness of Poincaré's approach (Lynden-Bell & Wood 1968; Katz 1978, 1979) than has the mechanics community, whose awareness is growing (Thompson 1979, Maddocks 1987, Lowry & Steen 1995, Luzzatto-Fegiz & Williamson 2012). Brown & Scriven (1980b) considered the shape and stability of rotating drops held by surface tension using the finite-element computational approach and, perhaps unsurprisingly, found numerous branching families of equilibria reminiscent of those summarized by Chandrasekhar (1987). Brown & Scriven (1980b) computed stability by direct evaluation of the second variation.

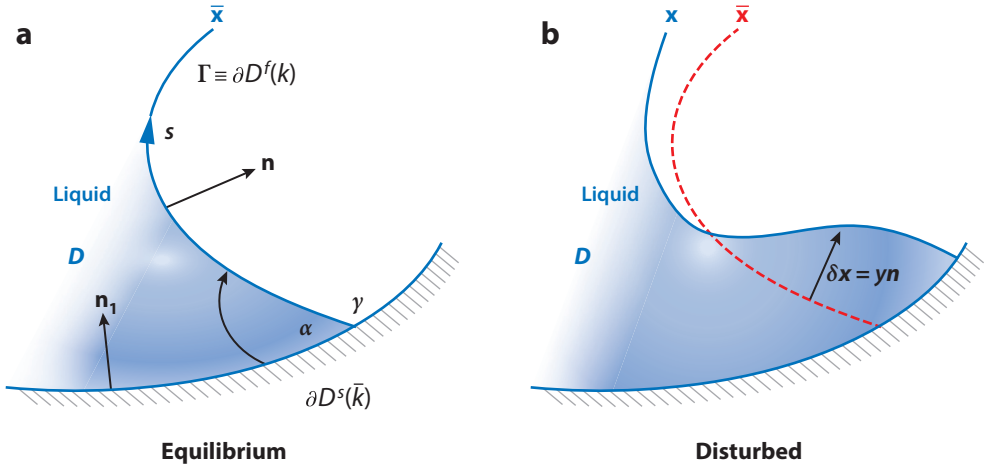

Figure 4

Region near contact line γ for a partially wetting liquid showing the (*a*) equilibrium (*blue solid line*) $\bar{\mathbf{x}}$ and (*b*) disturbed (*blue solid line*) $\mathbf{x} = \bar{\mathbf{x}} + \delta\mathbf{x}$ configurations with $\delta\mathbf{x} = y\mathbf{n}$. The capillary surface Γ, with normal curvature k and surface normal $\mathbf{n}$, intersects the solid support ∂D^s, with normal curvature $\bar{k}$ and surface normal $\mathbf{n}_1$, at the contact line γ to make the contact angle α.

One can treat the volume-conservation constraint as an auxiliary condition by introducing the Lagrange multiplier μ into an augmented functional,

$$F[\mathbf{x}] = U[\mathbf{x}] - \mu V[\mathbf{x}]. \tag{5}$$

2.2. Equilibrium (First-Order Conditions): Bulk, Surface, and Contact Line

For motionless base states, the pressure must be hydrostatic in the bulk. For negligible gravity, this implies a uniform pressure throughout.

The surface equilibrium conditions arise from the first variation of the energy functional. The capillary surface is perturbed, $\mathbf{x} = \bar{\mathbf{x}} + y\mathbf{n}$ (see **Figure 4**), and applied to the energy functional (Equation 5). The first variation requires that equilibria $\bar{\mathbf{x}}$ satisfy the first-order conditions

$$\frac{1}{\sigma}\delta F[\mathbf{x}] = \int_\Gamma (\kappa_1 + \kappa_2 - \mu)\, y\, d\Gamma + \int_\gamma (\mathbf{n}\cdot\mathbf{n}_1 - \cos\alpha)\frac{y}{\sin\alpha}\, d\gamma \tag{6}$$

for all allowable disturbances y. Here we note that the first-order conditions for the augmented functional $\delta F = 0$ are the same as those for the energy functional $\delta U = 0$ because of the volume-conservation constraint $\delta V = 0$.

A vanishing first variation, $\delta F = 0$, yields the equilibrium condition for the liquid/gas interface Γ,

$$\frac{p}{\sigma} = 2H \equiv \kappa_1 + \kappa_2 \quad [\partial D^f], \tag{7}$$

which relates the pressure p to the principal curvatures κ_1 and κ_2 there (Young 1805, Laplace 1806). For negligible gravity, Equation 7 implies that equilibrium surfaces have constant mean curvature H and belong to one-parameter families (see the sidebar Surfaces of Constant Mean Curvature).

Similarly, requiring $\delta F = 0$ delivers two alternative equilibrium conditions for the CL. The first is simply the pinned CL equation,

$$y = 0 \quad [\gamma], \tag{8}$$

SURFACES OF CONSTANT MEAN CURVATURE

Surfaces of constant mean curvature can be bounded or unbounded, singly or multiply periodic, self-intersecting or not. Delaunay (1841) gave a geometrical construction for all surfaces of revolution of constant mean curvature, classified by their curve of generation. These shapes are nodoids and unduloids, along with the special cases of the sphere, cylinder, and catenoid (Gillette & Dyson 1971). Along with the plane, these shapes exhaust the axisymmetric solutions to Equation 7 with constant H. Pieces of these shapes also constitute solutions. In addition, there are many unbounded constant H shapes without rotational symmetry. Block copolymers have been observed to undergo morphological changes between constant H configurations (Thomas et al. 1988, Jain et al. 2005). DNA structure motivates the study of the helicoid to catenoid ($H = 0$) transition, tested using soap films on a wire frame (Boudaoud et al. 1999). May & Lowry (2008) obtained the stability limits of volumes supported by dual helical boundaries, extending the work of Lowry & Thiessen (2007).

and the second is a geometric condition,

$$\mathbf{n} \cdot \mathbf{n}_1 - \cos\alpha = 0 \quad [\gamma], \tag{9}$$

relating the surface normals $\mathbf{n}$ and $\mathbf{n}_1$. Equation 9 is referred to as the natural boundary condition in the calculus of variations. Substituting $\cos\alpha = \mathcal{M}$ into Equation 9 yields the Young-Dupré equation in the surface-normal form (Young 1805, Dupré 1869).

2.3. Stability (Second-Order Conditions): Disturbance Classes

The stability of the equilibrium surface $\bar{\mathbf{x}}$ is determined by solving the eigenvalue problem associated with the second variation

$$\delta^2 F[y] \equiv -\Delta_\Gamma[y] - (\kappa_1^2 + \kappa_2^2)\, y - \mu y = \lambda y \quad [\partial D^f]. \tag{10}$$

Here y is the interface disturbance, and Δ_Γ is the Laplace-Beltrami operator or surface Laplacian, which is defined on the equilibrium surface,

$$\Delta_\Gamma[y] \equiv \frac{1}{\sqrt{g}} \frac{\partial}{\partial u^i} \left(\sqrt{g} g^{ij} \frac{\partial y}{\partial u^j} \right), \quad g_{ij} \equiv \bar{\mathbf{x}}_{,i} \cdot \bar{\mathbf{x}}_{,j}, \quad i, j = 1, 2 \quad [\partial D^f], \tag{11}$$

where g_{ij} is the surface metric tensor, using notation standard to differential geometry. Eigenvalues can be shown to be real (self-adjoint operator). The sign of the eigenvalue λ gives the stability of a particular mode; $\lambda > 0$ implies that the equilibrium is stable to that disturbance mode, whereas $\lambda < 0$ corresponds to instability. For the equilibrium to be stable, there can be no unstable modes. We note that, in the absence of symmetry, Equation 10 is a partial differential equation because disturbances take the form $y(u^1, u^2)$, where u^1 and u^2 are the surface coordinates.

Constraints on the bulk and at the CL influence stability, as mentioned in Section 1. For the bulk, one finds that either $\mu \neq 0$, corresponding to disturbances that preserve the volume, called volume disturbances, or $\mu = 0$, corresponding to disturbances of constant pressure, called pressure disturbances. For volume disturbances, one augments the second variation (Equation 10) with the following auxiliary condition on the function y to determine μ:

$$\int_\Gamma y \, \mathrm{d}\Gamma = 0 \quad [\partial D^f]. \tag{12}$$

PINNING CONTACT LINES IN PRACTICE

Pinning CLs in practice requires some combination of chemical and geometrical strategies. Several methods, some well based in prediction, are now part of the spacecraft engineer's toolbox. The most commonly used way to locate CLs under conditions of weightlessness is to introduce sharp corners (Langbein 2002, chapter 7), often by joining wedges of different materials to form the corner. The sharpness of the edges (the wedge angle) must satisfy specific conditions relative to the respective contact angles to be effective. Gibbs (1906) considered this problem and derived inequalities that hold when the CL coincides with a sharp edge of a solid support. Dyson (1988) raised objections to Gibbs's proof and provided a counterexample.

At the CL, for both volume and pressure disturbances, consistency with first-order conditions (Equation 6) requires either (*a*) a fixed CL (pinned CL) (Myshkis et al. 1987),

$$y = 0 \quad [\gamma], \tag{13}$$

or (*b*) a geometric condition (free CL),

$$y' + \chi y = 0, \quad \chi \equiv (k \cot\alpha - \bar{k}/\sin\alpha) \quad [\gamma], \tag{14}$$

where χ is a parameter related to the static contact angle α, the normal curvature k of the free surface, and the normal curvature $\bar{k}$ of the solid support (**Figure 4*a***). Disturbances to the free CL can behave as though pinned, $\chi \to \pm\infty$, or as preserving α, $\chi = 0$. In this way, one may think of χ as characterizing how easily a disturbance can be anchored, and Equation 14 suggests how chemical α and geometrical $\bar{k}$ modifications of a support surface compete or cooperate to pin a CL. In many applications, CL pinning is crucial, but doing so in practice remains largely an art (see the sidebar Pinning Contact Lines in Practice). We discuss how the geometry of the solid support affects stability in Section 3.2.2.

Direct computation of the spectrum λ of Equation 10 becomes challenging when it depends on multiple parameters. For volume disturbances $\mu \neq 0$, the computation is also complicated because one must enforce the auxiliary condition given in Equation 12. In this case, the Lagrange multiplier μ is treated as an additional parameter that must be determined as part of the solution, effectively increasing the system size. For example, Slobozhanin et al. (1997) and Myshkis et al. (1987) employed direct calculation to identify the critical disturbance for the liquid bridge with pinned CLs.

The conjugate-point method also directly computes stability. The focus is on the least-stable direction and its possible destabilization. The approach involves computing conjugate points of the Jacobi equation [the second variation (Equation 10) with $\lambda = 0$]. To prove stability, one must (*a*) satisfy Legendre's condition and (*b*) prove the absence of a conjugate point (Bolza 1904).

Poincaré-Maddocks (PM) method: stability changes are inferred from turning points and bifurcations in the preferred diagram

2.4. Poincaré Turning-Point Method

An alternative to direct computation is a TP method, which goes back to Poincaré (1885), with a modern treatment by Maddocks (1987), sometimes referred to as the Poincaré-Maddocks (PM) method. This bifurcation-theoretic approach extracts information from families of equilibria and thereby avoids solving Equation 10 directly. The advantage is considerable if one is primarily interested in changes in stability. The method is well suited to the isoperimetric nature of capillary

INDEX THEORY FOR ISOPERIMETRIC PROBLEMS

Underlying the PM theory is an index theory, related to the number of negative eigenvalues of the second variation on a constrained function space $\mathcal{S}$, that codifies the relationship between pressure and volume disturbances. The central idea is that the unconstrained (pressure) index $[\mathcal{U}]$ is simply related to the constrained (volume) index $[\mathcal{C}]$ through the following relationship, $[\mathcal{U}] = [\mathcal{C}] + [\mathcal{C}^{\perp}]$, where $[\mathcal{C}^{\perp}]$ is the index on the orthogonal complement to the constrained function space $\mathcal{S}^{\perp}$, which is related to the curvature of the augmented functional $\partial^2 F/\partial\lambda^2$ (Maddocks & Sachs 1995). The main PM theorem then follows immediately because the curvature, by definition, changes at a fold in the preferred diagram. Volume disturbances are relatively stable to pressure disturbances, as exhibited by the relationship between the constrained and unconstrained index.

surface problems (Lowry & Steen 1995) and to computational continuation (Doedel & Oldeman 2009).

We provide an example using the preferred diagram for a liquid bridge with equal pinned CLs (**Figure 5**). This family of equilibria, all pieces of Delaunay shapes, has been obtained by continuation in arc length along the branch, starting from the cylindrical bridge, just below B, and following in one direction and then reversing along the other direction. Three TPs appear: two extremals in pressure, between shapes A and B and between shapes B and C, and one in volume, between shapes C and D. PM theory states that the number of unstable eigenvalues λ (solutions to Equation 10) changes at TPs. Specifically, the stability index changes at the pressure TPs for pressure disturbances and at volume TPs for volume disturbances (see the sidebar Index Theory for Isoperimetric Problems). Because a cylinder of length $L = 2.72$ is stable to both pressure and volume disturbances (Plateau 1863), the starting point has indices $([p], [V]) = (0, 0)$. On decreasing volume, a pressure TP is first traversed to make the bridge pressure unstable $([p], [V]) = (1, 0)$ until beyond shape C, where the volume TP is then traversed and equilibria become volume unstable. Shape D is both pressure and volume unstable $([p], [V]) = (1, 1)$. In the other direction, index changes are similarly read off the response diagram. Using PM theory to infer stability changes is only useful when rotationally symmetric disturbances are most dangerous. This can sometimes be proved by Steiner symmetrization. That is, when symmetrization is possible, symmetric disturbances are most dangerous. The limiting shape at which the procedure ceases to work is the Steiner limit (see the sidebar Steiner Symmetrization).

Preferred diagram: a response diagram, according to the Poincaré-Maddocks prescription, that has the format of the isoperimetric (constrained) variable against the Lagrange multiplier (constraint) and consists of a family of equilibria

Stability index: the number of negative eigenvalues of the second variation when restricted to a particular disturbance class; an index 0 represents a stable equilibrium

STEINER SYMMETRIZATION

Steiner (1882) introduced a geometric procedure to map a three-dimensional shape onto a rotationally symmetric shape, preserving the volume while not increasing the surface area, which Gillette & Dyson (1972) proved for bridges with pinned CLs. This mapping procedure works, as long as the rotationally symmetric shape (and its three-dimensional disturbance) is single-valued in the radial coordinate of the cylindrical system. The limiting symmetric shape for a liquid bridge is therefore one that comes in tangent to the CL, which we call the Steiner limit. When constructible, the mapping proves that symmetric disturbances are most dangerous. When not constructible, there is no information. However, at least in the case of a liquid bridge, the Steiner limit also corresponds to the instability to azimuthal disturbances (**Figure 3*c***). Slobozhanin et al. (1997) proved this by solving Equation 10 at the Steiner limit. When symmetric disturbances are most dangerous, the second variation reduces to an ordinary differential equation for the function $y(u)$, a great simplification.

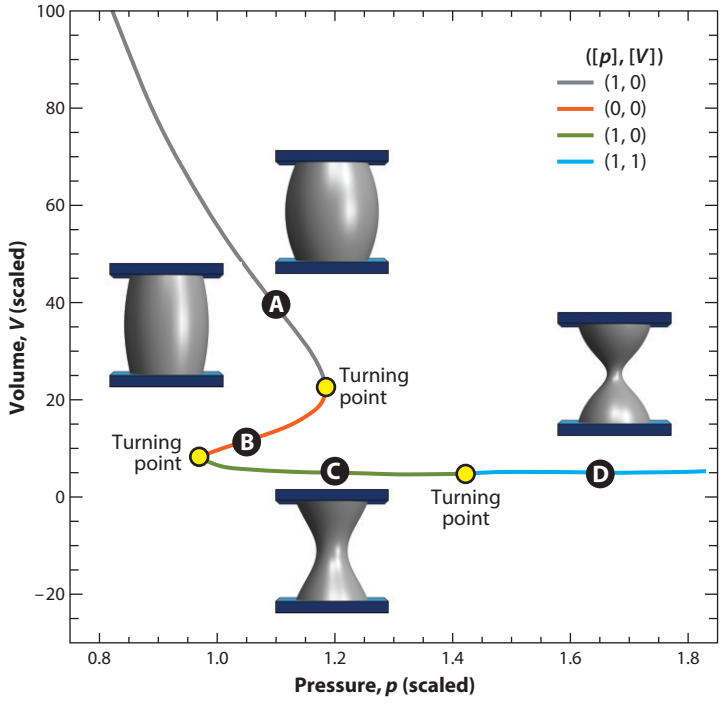

Figure 5

Pressure-volume response of a liquid bridge with a pinned contact line of scaled length $L = 2.72$. Rendered equilibrium shapes are labeled A–D. Stability changes, indicated by stability indices $[p]$ and $[V]$, occur at turning points (*yellow circles*) in pressure (between A and B and between B and C) and in volume (between C and D).

2.5. Systems: Compound Drops and Droplet Switches

Nowadays, double bridges, double drops, and other capillary systems are of interest for device design. Classically, they were of interest to test theory (Rücker 1886). In this section, using droplet systems, we illustrate the relevance of stability to design and, in the next, using compound bridges, we show how the PM method can be adapted to predict system stability.

Figure 6*a* illustrates a system of water drops undergoing a slow coarsening process. In the system is an array of 24 holes, drilled in a plate, with a reservoir attached beneath. Through a valve, a syringe overfills the reservoir until the 24 drops protrude as superhemispheres ($t = 0$ s in **Figure 6*a***). The valve is then closed so that the system, the drops and reservoir, has a fixed total volume. The initial state is unstable. As time progresses, owing to slightly varying initial curvatures (hence pressures), fluid is pumped to bigger drops, and the volume collects increasingly into fewer drops. After long-enough time, all excess volume ends up in a single drop ($t = 40$ s in **Figure 6*a***). The system has fully coarsened to an equilibrium state (neglecting evaporation). According to the theory of single-drop response (**Figure 1*c***), were they unconstrained, all n drops initially would be unstable as they fall on the upper branch. However, they must obey the overall volume constraint. Thus, the system may be thought of as having $n - 1$ rather than n degrees of freedom. The final rest state after 40 s in **Figure 6*a*** shows that 23 drops have behaved unstably, as if the stability were to pressure disturbances (unconstrained), whereas the big drop has behaved stably, as if responding to volume disturbances.

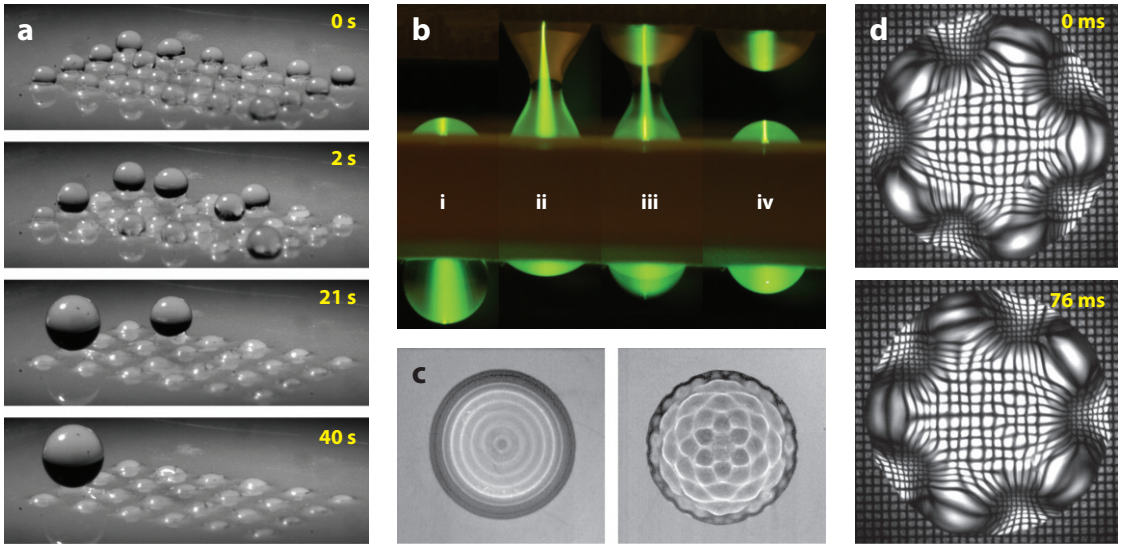

Figure 6

Dynamic instability. (*a*) Video images showing coupled drops coarsening in time, starting as 24 big drops of nearly equipartitioned volume (unstable equilibrium), $t = 0$ s, relaxing to six big drops at 2 s, to two big drops at 21 s, and to one big drop at 40 s, the final (stable) equilibrium. Panel *a* reproduced with permission from van Lengerich et al. (2010). (*b*) Time-sequence photos showing capillary switch (side view) toggling between droplet-droplet (*i*, *iv*) and droplet-bridge (*ii*, *iii*) configurations. Photographs courtesy of A. Hirsa. (*c*) Sessile drop (top view), mechanically excited (megahertz; $Oh \leq 0.003$), exhibiting (*left*) circular standing waves that, upon being shaken harder, lose symmetry to (*right*) asymmetric surface patterns. Panel *c* reproduced with permission from Vukasinovic et al. (2007). (*d*) Sessile drop (top view through a fixed mesh), mechanically excited (kilohertz; $Oh = 0.0024$), exhibiting a resonant mode [5, 5] at two instants one half period apart. Panel *d* reproduced with permission from Chang et al. (2013).

Regarding the coarsening of coupled water drops, a theory that predicts the instability of the initial state and the stability of the final state is available (Gillette & Dyson 1974, Slobozhanin & Alexander 2003). More generally, the theory predicts how the static stability of a system depends on the element stability. For n elements coupled in parallel with a system volume constraint $V = \sum_i^n V_i$, having all elements stable, $(dp/dV)_i > 0$, for $i = 1, \ldots n$, is sufficient for system stability but not necessary. Necessary conditions allow at most one element to take a configuration that would otherwise be unstable (i.e., as if uncoupled). Only under a certain additional condition do the necessary conditions become sufficient for system stability. This additional condition has been proved using a direct calculation of the second variation for coarsening of n drops coupled by various network topologies (van Lengerich et al. 2010), with relevance to the experiment just recounted. The related three-coupled drop instability has been treated by direct calculation from a catastrophe-theory perspective (Wente 1999).

Another example of the system behavior is provided by compounding two drops to form a double-welled energy landscape (Boys 1959 [1890]). When a means to toggle between the bistable states is introduced, a capillary switch is realized. Various toggling activations have been introduced, including acoustic (Hirsa et al. 2005), electro-osmotic (Vogel et al. 2005, Barz & Steen 2013), magnetic (Malouin et al. 2010), and electric fields (Sambath & Basaran 2014).

Figure 6*b* shows a 1-mm-thick plate in which a single hole has been drilled and then overfilled with fluorescein-laden water, illuminated by a laser sheet. In the static configuration (part i), pinned drops protrude above and below the plate, and the bistable state big-down is shown. Parts ii–iv in **Figure 6*b*** show snapshots of the switch during toggling against a second plate,

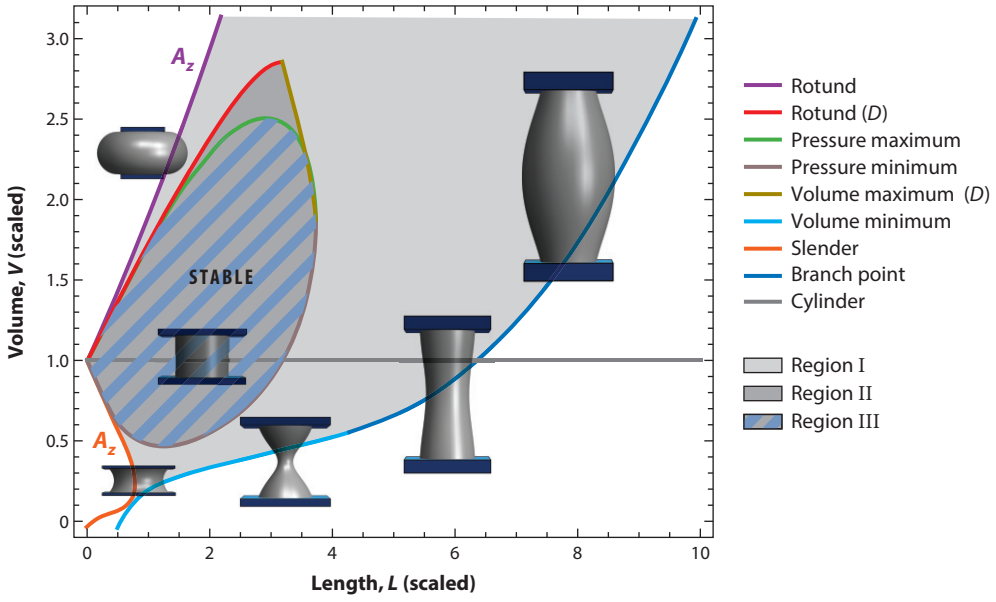

Figure 7

Stability windows: boundaries of stable regions, in volume-length (*VL*) space, for a single liquid bridge with pinned CLs for volume (*region I*) and pressure (*region III*) disturbances and for a dual-bridge (*D*) system for a fixed total volume (*region II*). The instability at boundaries is to rotationally symmetric modes except at rotund and slender limits in which azimuthal (A_z) modes are most dangerous. Rendered shapes along boundaries are those before instability. A shape at the Steiner limit, azimuthally unstable, is shown in the upper left. Lengths are scaled by pinning CL radius, and volumes by the cylindrical volume.

positioned above. Activation occurs by an acoustic pulse applied to the lower chamber. In part iii, the up state is overshot, and a liquid bridge forms momentarily until, on rebound (part iv), it breaks, leaving a droplet above. In this way, the bridge grabs the top plate and then releases it.

Vogel & Steen (2010) reported an electronically controlled adhesion device based on this grab-and-release action. The device arranges hundreds of droplet switches to act in parallel, toggled by electro-osmotic activation. Bistability is crucial to the design in that no power is needed to maintain either the grabbed or released state, only to toggle between. In another application, in which the pinning of droplets is essential, López et al. (2005) tested a variable focal-point lens that dynamically varies the curvatures of the droplets in the switch.

2.6. Stability Window: Singlet and Dual Bridges

Axisymmetric mode or shape: mode or disturbance shape that possesses rotational symmetry about a generating axis

A stability window can be constructed from response diagrams. For the singlet bridge, we start with the TPs in **Figure 5**. **Figure 7** plots the locus of the three TPs, the pressure maximum and minimum and the volume minimum, as *L* varies. The pressure limits form a closed loop, yielding the window of stability to pressure disturbances. The window to volume disturbances comprises the volume limit (by PM theory), supplemented by the branch point curve (large lengths), and the slender and rotund limits for small lengths. The slender and rotund limits are to azimuthal disturbances (A_z), which occur at the Steiner limit and are therefore not picked up by the PM response diagram, which assumes rotational symmetry. In summary, the full stability window for the pinned singlet bridge, to both pressure and volume disturbances, can be obtained using PM theory to locate axisymmetric instabilities, tracing the TPs in the secondary parameter

L and combining rotationally symmetric limits with the Steiner limits (Lowry & Steen 1995). The rotationally symmetric limits in **Figure 7** were first obtained by solving Equation 10 using the conjugate point method (Hormann 1887, Howe 1887) to which the Steiner limits were added (Gillette & Dyson 1971). More recently, Slobozhanin et al. (2012) obtained the bifurcation structures along the edges of the stability window, computing with a weakly nonlinear extension of Equation 10.

The stability window for a dual-bridge system can be obtained using PM theory in much the same way. The dual-bridge pressure-volume response is easily constructed graphically from the singlet response (**Figure 5**), as $V \equiv V_1 + V_2$, and equilibrium requires $p_1 = p_2 \equiv p$. That is, the system response will have a trunk branch that is identical to the element response but with twice the volume. These states are identical twins. From that trunk, additional branches (nontwins) will bifurcate into the fold direction at each pressure TP. This occurs because, whenever the response in **Figure 5** is triple-valued, there are three choices for V_1 and V_2 for every p.

A conventional bifurcation diagram can be obtained by replotting the response diagram as $V_2 - V_1$ against V, in which bifurcations are seen to be pitchforks. PM theory can be used to find the relative stability of each branch. TPs are obtained by introducing an imperfection to break the bifurcations. Applying the PM rules to the imperfect bifurcation yields the set of stability changes. The response can then be deformed back to the perfect state, a deformation that preserves stability changes (Lowry & Steen 1995). The relative stability of all branches is thereby fully resolved. From these, the stability window can then be assembled, as described for the singlet bridge. The resulting dual-bridge limits consist of pressure-minimum, volume-maximum, and rotund curves (**Figure 7**), extending the single-bridge pressure stability window in the direction of larger volumes.

In summary, three stability windows are nested in **Figure 7**. The pinned singlet bridge subject to volume disturbances, having the largest window, is the most stable; the dual bridge to volume disturbances is the next most stable; and the singlet bridge to pressure disturbances, having the innermost window, is the least stable. Coupling the bridges makes them behave like pressure-disturbed singlet bridges subject to some stabilizing influence by the system's volume constraint. This stabilization can be traced back to the birth, on coupling, of the nontwin branch at the maximum pressure TP, most clearly seen in the graphical PM approach.

3. HYDRODYNAMIC STABILITY: A PARALLEL FORMALISM

In this section, we establish the parallels between the static and hydrodynamic formulations. For the dynamic formulation, one must solve for the disturbance velocity $\mathbf{v}$ and pressure p fields everywhere in the fluid domain. Normal modes $e^{i\lambda t}$ are invoked, which reduces the variables to time independent, and the flow problem (interior domain) is mapped onto the undisturbed interface using Green's functions, a boundary-integral approach. Here the frequency λ is scaled by a capillary timescale $\sqrt{\rho l^3/\sigma}$, with ρ the fluid density and l the characteristic length scale. For brevity, we assume that the underlying fluid is inviscid and define the velocity field $\mathbf{v} = \nabla\phi$ through the reduced velocity potential ϕ for irrotational flow. [Inviscid analyses and extensions accounting for viscous effects and vorticity are reported for liquid bridge vibrations (Borkar & Tsamopoulos 1991, Kidambi 2011) and for belted-sphere oscillations (Bostwick & Steen 2013a,b).] One can then write the linearized hydrodynamic field equations as an eigenvalue problem,

$$-\Delta_\Gamma\left[\frac{\partial\phi}{\partial n}\right] - \left(\kappa_1^2 + \kappa_2^2\right)\left(\frac{\partial\phi}{\partial n}\right) = \lambda^2\phi \quad [\partial D^f], \tag{15}$$

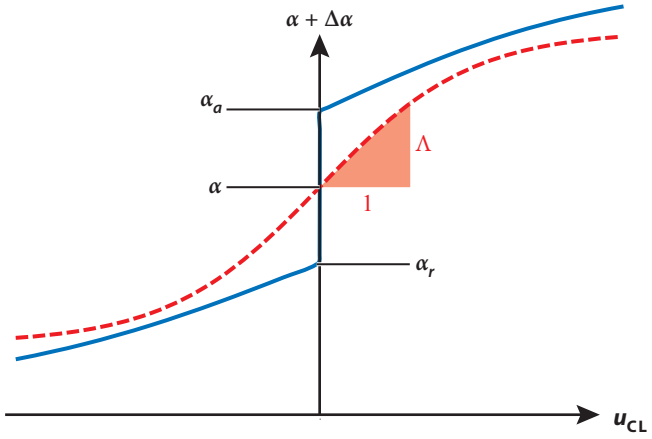

Figure 8

Schematic illustration of contact-line speed u_{CL} versus angle α, with advancing α_a and receding α_r static contact angles (*solid lines*). Shown is a model of the continuous-speed condition $\Delta\alpha = g(u_{\mathrm{CL}})$ (*dotted line*) with mobility resistance parameter Λ, having limits that recover the free, $\Lambda = 0$, and pinned, $\Lambda = \infty$, contact-line conditions. Figure after Davis (1980).

which is augmented with a CL boundary condition on γ and auxiliary conditions as follows:

$$\nabla^2\phi = 0 \quad [D], \qquad \nabla\phi \cdot \mathbf{n}_1 = 0 \quad [\partial D^s], \qquad \frac{\partial\phi}{\partial n} = i\lambda y \quad [\partial D^f], \qquad \int_\Gamma \frac{\partial\phi}{\partial n} d\Gamma = 0 \quad [\partial D^f]. \tag{16}$$

In other words, the reduced velocity potential must satisfy Laplace's equation on the fluid domain D, the no-penetration condition on the solid support ∂D^s, a kinematic condition on free surface ∂D^f that relates the velocity field to the interface disturbance there (see **Figure 4**), and the overall volume constraint. We note the parallel structure of Equations 10 and 15. In the static case (Equation 10), $\lambda < 0$ corresponds to unstable directions (modes) in the function space, whereas, in the hydrodynamic case (Equation 15), $\lambda^2 > 0$ corresponds to oscillations. For oscillatory instability, higher modes can be excited and observed. For static stability, special control is needed to observe a higher unstable mode (Thiessen et al. 2002). Typically, only the most unstable mode can be observed.

As in the case of static stability, the disturbance behavior at the CL greatly affects dynamic stability. CL motion is accommodated by a constitutive law, $\Delta\alpha = g(u_{\mathrm{CL}})$, that relates the contact angle deviation $\Delta\alpha$ smoothly to the CL speed u_{CL} as hysteresis is not compatible with the linear analysis (**Figure 8**). Linearizing about the static base state $u_{\mathrm{CL}} = 0 + \epsilon(\partial\phi/\partial n)$ gives the following generalization of Equation 14,

$$\left(\frac{\partial\phi}{\partial n}\right)' + \chi\left(\frac{\partial\phi}{\partial n}\right) = i\lambda\Lambda\left(\frac{\partial\phi}{\partial n}\right) \quad [\gamma], \tag{17}$$

with differentiation with respect to the arc-length coordinate, $' = d/ds$. This CL condition was introduced by Davis (1980), although it is sometimes referred to as the Hocking condition, even though Hocking (1987) attributed it to Davis. Here $\Lambda \equiv g'(0)$ is a mobility resistance parameter (see **Figure 8**). This parameter can be used to smoothly change the boundary conditions between fully mobile (Equation 14), $\Lambda = 0$, and pinned (Equation 13), $\Lambda = \infty$, CLs. The intent here is a phenomenological means to account for CL motion, not a molecular-based model. One

can think of Λ as a tuning parameter to interpolate between extremes. Reviews of moving CLs include Dussan V. (1979), de Gennes (1985), and Snoeijer & Andreotti (2013).

3.1. Operator Equation and Disturbance Energy

To unify the formalism, we recast the eigenvalue problem given by Equation 15 as an operator equation,

$$\lambda^2 M\left[\frac{\partial\phi}{\partial n}\right] = K\left[\frac{\partial\phi}{\partial n}\right] \quad [\partial D^f]. \tag{18}$$

Here M is an integral operator representative of the fluid inertia, and K is a differential operator related to the curvature:

$$M\left[\frac{\partial\phi}{\partial n}\right] \equiv \phi, \quad K\left[\frac{\partial\phi}{\partial n}\right] \equiv -\Delta_\Gamma\left[\frac{\partial\phi}{\partial n}\right] - (\kappa_1^2 + \kappa_2^2)\left(\frac{\partial\phi}{\partial n}\right). \tag{19}$$

To proceed with this formulation, one must construct a sufficiently general solution to the boundary value problem, where the volume constraint is incorporated into the Green's function for the inverse of K,

$$\nabla^2\phi = 0 \quad [D], \quad \frac{\partial\phi}{\partial n} = f_k \quad [\partial D^f]. \tag{20}$$

More specifically, given a surface deformation f_k, one needs to compute the corresponding velocity potential ϕ_k, in accordance with the inertia operator M. For this reason, capillary instability flows are referred to as interfacially driven flows.

Taking the inner product, $(f, g) \equiv \int_\Gamma fg\, d\Gamma$, of Equation 18 with $\partial\phi/\partial n$ yields the disturbance energy equation,

$$\lambda^2\left(M\left[\frac{\partial\phi}{\partial n}\right], \frac{\partial\phi}{\partial n}\right) = \left(K\left[\frac{\partial\phi}{\partial n}\right], \frac{\partial\phi}{\partial n}\right) \quad [\partial D^f]. \tag{21}$$

Minimizers of the functional

$$\mathcal{L}[y] \equiv (K[y], y)/(M[y], y) \tag{22}$$

are necessarily solutions of the governing equations (Equation 15), provided the auxiliary conditions (Equation 16) are satisfied (Myshkis et al. 1987). The no-penetration constraint can be either (*a*) built into the function space or (*b*) introduced to the disturbance energy via Lagrange multipliers. The spectrum can be computed via a Galerkin projection of the operator equation (Equation 18) or by the Rayleigh-Ritz method. In the latter, one applies a solution series, $y = \sum_{j=1}^{N} c_j y_j$ with y_j basis functions, to the functional and minimizes with respect to the coefficients c_j to obtain a set of algebraic equations. Bostwick & Steen (2013a) restricted y_j, illustrating method (*a*), whereas Bauer & Chiba (2004) and Vejrazka et al. (2013) used Lagrange multipliers, illustrating method (*b*).

3.2. Spectral Ordering and Modal Monotonicity: Relative Stability

Eigenvalue solutions to self-adjoint operator equations, such as Equation 18, vary with problem parameters. This variation can often be predicted a priori. Here, we paraphrase relevant theorems (Courant & Hilbert 1953) and their implications, restricting the discussion to volume disturbances with pinned ($\Lambda = \infty$) or mobile ($\Lambda = 0$) CL conditions, the limiting cases of Equation 17. These make precise the rule of thumb that constraint increases frequency, for example. In view of the parallel formalism, these results hold for both static (Equation 10), with M replaced by the identity operator I in Equation 22, and hydrodynamic (Equation 18) problems.

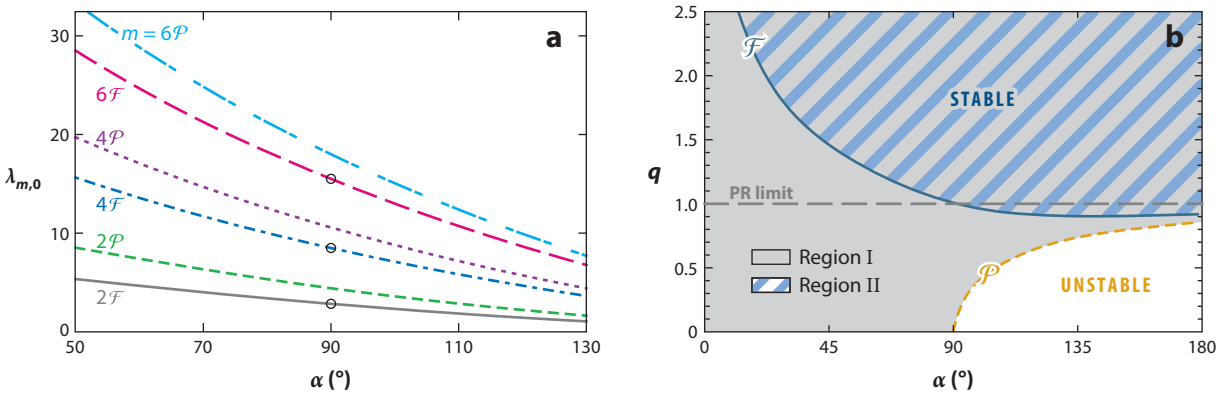

Figure 9

Spectral ordering and modal monotonicity. (*a*) Sessile drop natural frequency $\lambda_{m,0}$ for the first three axisymmetric modes (polar wave numbers $m = 2$, 4, and 6) against contact angle α for free, $\mathcal{F}$, and pinned, $\mathcal{P}$, disturbances. Circles mark Rayleigh-Lamb frequencies. (*b*) Static rivulet stability window, axial wave number q against contact angle α, for free (*region II*), $\mathcal{F}$, and pinned (*region I*), $\mathcal{P}$, disturbances. For free disturbances, the stability window widens with α (narrows with cosα). The Plateau-Rayleigh (PR) limit (*gray dashed line*) is shown for reference. For both the rivulet and drop, pinning stabilizes, consistent with spectral ordering.

3.2.1. Spectral ordering. Let λ_n and μ_n be the n-th eigenvalue solutions of Equation 10 or 18 for the pinned, $y = 0$, and fully mobile, $\partial y/\partial n + \chi y = 0$, CL conditions, respectively. Then, one obtains $\mu_n \leq \lambda_n$.

If an equilibrium surface is stable to free disturbances, then it must also be stable to pinned disturbances. Equivalently, if a surface is unstable to pinned disturbances, it must also be unstable to free disturbances.

For the static problem, this makes precise the effect of $\delta A_{ls} = 0$ on the minimizers of the functional (Equation 2), discussed in Section 1. Examples include the nested stability windows for the static rivulet (Davis 1980) reproduced in **Figure 9*b***. The stability window for the free CL is nested within that for the pinned CL.

For the dynamic problem, this is illustrated in the oscillatory spectrum for the sessile drop in the case of a hemisphere (Lyubimov et al. 2006) and for the more general case of a spherical cap (Bostwick & Steen 2014) (**Figure 9*a***).

Relatedly, among admissible disturbances, those that satisfy the natural boundary conditions (Equation 14) are absolute minimizers of Equation 22. That is, the fully mobile disturbance is the most destabilizing disturbance that a capillary surface can be subjected to. Equivalently, it is the least constrained (or most unconstrained) disturbance. This is used to identify the appropriate disturbance class (function space) when solving CL conditions such as Equation 17 that are neither pinned nor mobile (discussed below).

Free disturbance: disturbance having a free contact line; also referred to as a natural disturbance in the calculus of variations

Pinned disturbance: disturbance having a fixed or immobile contact line

3.2.2. Modal monotonicity. For the natural boundary condition $\partial y/\partial n + \chi y = 0$, eigenvalue solution λ_n of Equation 10 or 18 only change in the same sense as the function χ, where we recall that $\chi \equiv (k \cot\alpha - \bar{k}/\sin\alpha)$. Eigenvalues vary monotonically with χ, mode-wise (i.e., for fixed n).

For fixed interface shape k, α, a concave solid support ($\bar{k} < 0$) is relatively stable to a planar support ($\bar{k} = 0$), which is relatively stable to a convex support ($\bar{k} > 0$). With regards to **Figure 2**, this demonstrates that the liquid bridge configuration shown in **Figure 2*e*** is relatively stable to that in **Figure 2*b***. Or, regarding the far-left column of the figure, free drop configurations become more stable from the bottom to top. Varying $\bar{k}$ is a homotopy.

Another implication is that, for an interface in contact with a planar support $\bar{k} = 0$, relative stability can be inferred from the sign of $\chi = k \cot \alpha$. For the sessile drop, one obtains $\chi = \cos \alpha$, and eigenvalues decrease with increasing α, as in **Figure 9*a*** (Bostwick & Steen 2014).

3.3. Dynamic Contact Line and Davis Dissipation

The disturbance energy balance for the CL speed condition (Equation 17) follows similarly to Equation 21:

$$\lambda^2 \left(M \left[\frac{\partial \phi}{\partial n} \right], \frac{\partial \phi}{\partial n} \right) + i\lambda\Lambda \int_\gamma \left(\frac{\partial \phi}{\partial n} \right)^2 \mathrm{d}\gamma - \left(K \left[\frac{\partial \phi}{\partial n} \right], \frac{\partial \phi}{\partial n} \right) = 0 \quad [\partial D^f]. \tag{23}$$

On introducing the CL speed condition, Davis (1980) showed that CL motion is purely dissipative for $\Lambda \neq 0$ (see **Figure 8**), pointing out the formal similarity of Equation 23 to the characteristic equation of a damped harmonic oscillator. To distinguish from viscous dissipation, we refer to this as Davis dissipation. For the free and pinned disturbances, there is no dissipation (Myshkis et al. 1987, Benilov & Billingham 2011). We note that introducing Equation 17 breaks the self-adjoint property of Equation 21, and λ^2 will no longer be necessarily real. Lyubimov et al. (2006) showed that the oscillation frequency for the hemispherical drop increases monotonically with Λ from $\Lambda = 0$ (free) to $\Lambda = \infty$ (pinned), whereas the decay rate achieves a maximum at a finite value of the mobility parameter and tends toward zero in the limiting cases $\Lambda = 0, \infty$. Bostwick & Steen (2014) considered the more general spherical-cap drop, recovering the results of Lyubimov et al. (2006) regarding Λ dependence.

3.4. Sessile Drops

Rayleigh (1879) solved Equations 15 and 16 to show that a free drop (with Γ being a sphere) oscillates with characteristic frequencies

$$\lambda_m^2 = m(m-1)(m+2), \quad m = 0, 1, \ldots, \tag{24}$$

and mode shapes P_m given by the Legendre polynomials. We refer to Equation 24 as the Rayleigh spectrum. Lamb (1932) noted that the Rayleigh spectrum is degenerate. For every $m > 0$, there are distinct spherical harmonics mode shapes Y_m^l, with the same frequency $\lambda_{m,l}^2 = m(m-1)(m+2)$ with $l \leq m$, which we call the Rayleigh-Lamb (RL) spectrum. Azimuthal ($l \neq 0$) mode shapes Y_m^l are not included in the axisymmetric Rayleigh modes $Y_m^0 \equiv P_m$.

Sessile drops with $\alpha = 90°$ and mobile CLs ($\Lambda = 0$) have RL modes provided that the sum of $m + l$ is even as these mirror-symmetric disturbances satisfy the no-penetration condition on the mid-plane (Equation 16). These modes of course inherit the azimuthal degeneracy of the RL spectrum. Pinning raises the frequency of these sessile drops (see **Figure 9*a***), consistent with spectral ordering (see Section 3.2.1). Bostwick & Steen (2014) extended the results of Lyubimov et al. (2006) to both sub- and superhemispherical base states. Basaran & DePaoli (1994) previously calculated the frequency of the lowest-wave-number axisymmetric mode (an extension of the $[m, l] = [2, 0]$ RL mode) for pinned drops as it varies with α, using finite-element simulations. Recent predictions are in agreement with these prior computations.

For a hemispherical drop, Lyubimov et al. (2004) showed that the spectral degeneracy is broken by varying the mobility parameter $\Lambda \neq 0$. Frequencies split for modes with fixed m, increasing with the azimuthal wave number l. Asymmetric modes have been observed on gradient surfaces (Daniel et al. 2004), air cushions (Noblin et al. 2005), and pressure-driven drops (Sharp et al. 2011). Recent observations by Chang et al. (2013) of mechanically oscillated, sessile water droplets catalogued

Rayleigh spectrum: the frequencies (Equation 24) at which a free capillary drop oscillates, with corresponding mode shapes given by the Legendre polynomials

Rayleigh-Lamb (RL) spectrum: the frequencies (Equation 24) at which a free drop oscillates, with additional azimuthal mode shapes given by the spherical harmonics

PERIODIC TABLE OF MODE SHAPES

The nature of the eigenvalue problem for a sessile drop (Equation 15) invites a comparison to the classic symmetry-breaking properties of the Schrödinger equation. The Schrödinger equation is an eigenvalue problem with spherical symmetry for the hydrogen atom (*s* orbitals) that gets broken systematically with higher atoms having less symmetry (*p*, *d*, and *f* orbitals). This symmetry breaking leads to splitting of the eigenvalues (splitting of spectral lines). For a sessile drop, Equation 15 also starts with spherical symmetry (the Rayleigh spectrum) and has subsequent splitting as the support plane is introduced. The drop degeneracy may be broken by (*a*) the spreading parameter Λ and (*b*) the base-state volume via the static contact angle α (Bostwick & Steen 2014). For certain values of these symmetry-breaking parameters, two modes may share the same characteristic frequency, or the classical ordering of modes can be altered. To organize and explain the hierarchy of frequencies, one can construct a corresponding periodic table of mode shapes using an Aufbau principle, in which modes are filled in order of increasing frequency.

the first 37 modes arising from the spectral splitting. The [5, 5] mode is shown in **Figure 6*d***. In summary, the RL spectrum, $\alpha = 90°$, is found to be largely inadequate as an approximation to the $\alpha \neq 90°$ spectrum for droplets with $\Lambda = \infty$. In fact, for large deviations from $\alpha = 90°$, we showed that spectral reordering may occur (Bostwick & Steen 2014) (see the sidebar Periodic Table of Mode Shapes).

3.4.1. Low-frequency motions and constraint: the Noether mode. The $m = 1$ mode of the Rayleigh spectrum is a zero-frequency mode related to translational invariance. Translational invariance ensures a first integral of the motion by Noether's theorem. Accordingly, we refer to $m = 1$ modes as Noether modes (either $[m, l] = [1, 0]$ or $[m, l] = [1, 1]$, as admissible). Strani & Sabetta (1984) broke the translational invariance by constraining the free drop to contact a spherical-bowl support (**Figure 2*a***). The constraint introduces a new low-frequency oscillatory mode, related to the zero-frequency [1, 0] Noether mode of the Rayleigh spectrum, that correlates with center-of-mass motion. The low-frequency prediction compares well with experiments by Bisch et al. (1982).

Similar to the bowl support, a pinned circle of contact also generally introduces a low-frequency mode linked to the Noether mode. Bostwick & Steen (2009) reported that the center-of-mass motion is partitioned among all the eigenmodes, but the low-frequency mode is its principal carrier. If the support circle is placed exactly on a nodal line of a spherical drop, there is of course no influence on the frequency. Otherwise, there is an influence. Ramalingam et al. (2012) and Prosperetti (2012) studied the same problem, both essentially using a Lagrange multiplier method to enforce the no-penetration condition at the pinning circle. Ramalingam et al. (2012) explicitly used Lagrange multipliers, whereas Prosperetti (2012) introduced a singular pressure, whose coefficient is determined from the no-penetration condition. Both methods allow for a kink (a discontinuous derivative) in the interface shape at the circle of contact. Bostwick & Steen (2013a) made this disturbance class explicit and showed that a mode with the discontinuous derivative always has a lower frequency than that with a continuous derivative. If the disturbance class (function space) is overly narrow, as when kinks are not allowed at pinning sites, then the frequency will be overpredicted. Increasing the extent of support from a pinning circle to a spherical belt increases the natural frequency, mode-wise, provided the location of the initial pinning circle remains fixed (Bauer & Chiba 2004, Bostwick & Steen 2013a).

Yet another drop constraint is related to the Noether mode. One can obtain coupled spherical-cap surfaces by introducing a spherical belt (**Figure 2*b***), centered on the equator with

the bowl removed. This is related to the capillary switch, discussed above, shown in part i of **Figure 6*b***. Theisen et al. (2007) assumed spherical-cap shapes to model the large-amplitude natural oscillations of the center of mass for the coupled droplet system. Ramalingam & Basaran (2010) employed finite-element simulations to determine the time-dependent response (frequencies, flow fields) of the double-droplet system to (*a*) pressure forcing and (*b*) solid substrate oscillations. The low-frequency mode, a relative of the Noether mode, is featured in these studies.

3.4.2. Mobile contact line. Lyubimov et al. (2006) applied the speed condition (Equation 17) to the hemispherical ($\alpha = 90°$) base state and reported damped oscillations for $0 < \Lambda < \infty$. They showed that the lower-wave-number modes dissipate more energy over an oscillation cycle because they have larger CL displacement, consistent with Equation 23. Fayzrakhmanova & Straube (2009) considered a hemispherical drop subject to forced oscillations. They applied a piecewise speed condition, which admits finite contact-angle hysteresis, and considered a small-displacement limit to capture stick-slip behavior at intermediate values of Λ. Stick-slip behavior is central to droplet-transport experiments that exhibit ratcheting motion (Daniel et al. 2004; Noblin et al. 2004, 2009).

Bostwick & Steen (2014) varied both the contact angle α and the mobility of the CL. Their results compare favorably to experiments (Sharp et al. 2011, Sharp 2012, Chang et al. 2013). They predicted how the mobility will affect the spectrum of the vibrated pinned sessile drops.

For piezoelectrically driven drops, Vukasinovic et al. (2007) reported an azimuthal instability, a transition to nonaxisymmetry, related to CL depinning, as suggested in **Figure 6*c***. In addition to affecting the spectrum, CL constraints such as those employed by Mampallil et al. (2011) can enhance mixing in oscillating droplets. Electrowetting techniques have similarly been used to induce CL motion to amplify flow and enhance mixing (Ko et al. 2008, Oh et al. 2008).

3.4.3. Walking drop instability. In view of $\lambda^2 > 0$ for the Rayleigh spectrum, all sessile-drop motions might be expected to be oscillatory. However, a sessile drop with a fully mobile CL is unstable to the Noether [1, 1] mode for $\alpha > 90°$,which might have been anticipated by modal monotonicity (Section 3.2.2). We showed that the walking instability occurs by a decrease in both surface areas, A_{ls} and A_{lg} (Bostwick & Steen 2014). Walking correlates with a horizontal center-of-mass motion. That an azimuthal mode can lower the overall surface energy may be surprising. However, in a recent study of the static stability of a free droplet sitting atop the flat end of a supporting rod, Muralidharan et al. (2013) reported an azimuthal shape that yields a lower overall energy $\mathcal{A}$ (Equation 2).

3.5. Bridge Vibrations

Liquid bridge oscillations, natural and forced, parametric and otherwise, have been of interest to the microgravity science community for some time. Interest in float-zone processing of materials in low gravity initially stimulated the activity. The influence of thermocapillarity on bridge stability also received considerable attention. Stability analyses and low-gravity experiments through the 1980s are nicely summarized by Langbein (2002, chapter 12). Since then, there has been considerable progress in solving the stability problem for quiescent base states of cylindrical shape. Much of the focus has been on viscous oscillations, usually with gravity small or neglected. Tsamopoulos et al. (1992) restricted the focus to axisymmetric disturbances and reported resonant frequencies and damping rates for a range of moderate to high Reynolds numbers. Chen & Tsamopoulos (1993) then reported the influence of nonlinearity for forced and free vibrations, and Mollot et al.

(1993) compared prediction to experiment. Finally, Kidambi (2011) included the azimuthal disturbances to complement Tsamopoulos et al.'s (1992) earlier study. All these modeling studies assume pinned CLs on the end supports.

From the viewpoint of this review, the most interesting results emerge from the mobile CL paper that begins this series. Borkar & Tsamopoulos (1991) solved the linear inviscid problem, essentially Equation 15 using the speed condition in Equation 17 controlled by a mobility parameter. They supplemented their inviscid solution with corrections for the viscous boundary layers that occur near the end supports and the weaker ones that occur near the free surface. They observed that (*a*) as the CL behavior varies between being pinned and free, the damping peaks near the location at which the frequency steps down from its constrained to unconstrained limit; (*b*) the damping due to Davis dissipation at the CL is more significant than that due to viscosity at high-enough Reynolds numbers; and (*c*) damping is negative for a range of mobilities. Observation (*a*) is consistent with the mobile drop behavior discussed above. Moreover, observation (*b*) suggests the importance of Davis dissipation. Finally, observation (*c*) is suggestive of the instability growth associated with the walking drop instability and consistent with reports by Hocking (1987). Borkar & Tsamopoulos (1991) struggled to interpret the negative damping and suggested that it deserved further study. Pinned CLs were used in all their subsequent studies.

3.6. Rivulets

A rivulet is a constrained liquid cylinder in much the same way that a sessile drop is a constrained spherical drop. Starting with a free cylinder, let us imagine just touching a planar support to the cylinder so that a line of contact is established. Davis (1980) showed that this simple constraint stabilizes the unconstrained cylinder (the PR limit). In terms of an axial wave number, if $q_c = 1$ corresponds to the PR limit, then $q_c = (3/4)^{1/2}$ is the new limit with the line-of-contact support. If the support plane intersects the cylinder at a contact angle α along the two straight parallel CLs, assumed pinned, then the stabilization of the constraint is given by

$$q_c^2 = 1 - \pi^2/(2\alpha)^2. \tag{25}$$

This stability boundary is plotted in **Figure 9*b***. This pinned result was anticipated by Brown & Scriven (1980a), who evaluated Equation 10 directly, and was corroborated by Bostwick & Steen (2010), who recovered the limit from a hydrodynamic analysis for a rivulet constrained by a cylindrical-cup support. Closely related is the meniscus stability on a variety of support geometries for pinned disturbances. There is a large number of studies on cylindrical interfaces. For example, Langbein (1990) studied the interior or exterior wetting of a V-groove, Roy & Schwartz (1999) analyzed a number of cross-sectional containers (e.g., planar, V-groove, circular, and elliptical), and Benilov (2009) used lubrication theory to treat a pendant rivulet. In each case, the critical disturbance is the axisymmetric varicose mode.

In contrast, mobile CLs are destabilizing to the static rivulet, consistent with the discussion in Section 3.2.2. **Figure 9*b*** shows that for $\alpha < 90°$, shorter rivulets can be destabilized; that is, the stability window shrinks relative to the free cylinder (Davis 1980). We solved the hydrodynamic stability problem for a static rivulet with mobile CLs. Although the varicose mode is the dominant mode, a sinuous (asymmetric) instability also exists, growing at a slower rate.

A rivulet with an axial base flow is susceptible to kinematic-wave instabilities characteristic of thin-film flows, especially if the rivulet is relatively flat. Weiland & Davis (1981) and Young & Davis (1987) studied the long-wavelength varicose instabilities of a rivulet with unidirectional gravity-driven flow down a vertical plane and reported capillary instability for narrow rivulets and kinematic-wave instabilities for wide rivulets. Rivulet meandering (sinuous instability) is not as

well understood as capillary breakup of rivulets and has been the subject of several experimental studies (Schmuki & Laso 1990, Nakagawa & Scott 1992, Nakagawa & Nakagawa 1996). Culkin & Davis (1983) derived a stability index to measure the stabilizing effects of surface tension and the destabilizing effects of inertia under dynamic wetting conditions. Their stability index was only marginally effective at capturing the observed meandering instability, partly because of the inability to model contact-angle hysteresis. Kim et al. (2004) studied a rivulet with a plug-flow base state and used a perturbation analysis to capture the meandering instability. By balancing pressures at the CL, they found a dispersion relation that depends on the base-state geometry, a Weber number, and wetting conditions on the CL. Similarly, Grand-Piteira et al. (2006) derived a meandering-rivulet criterion from a force balance on the CL that incorporates contact-angle hysteresis, capillary effects, and inertia from a gravity-driven base flow. Among other results, they found that the base flow is also hysteretic, and thus the shape of the meandering rivulet varies only with increasing flow rate. In each case, inertia competes with wetting and CL mobility to influence the character of the dominant instability.

3.7. Capillary-Gravity and Faraday Waves

Closely related to drops, rivulets and bridges are liquids having a planar free surface, contained laterally. The stability of these capillary surfaces belongs to the study of capillary-gravity (Lamb 1932) and Faraday (1831) waves. For details, we refer the reader to the reviews by Miles & Henderson (1990) and Perlin & Schultz (2000), noting that many of the methods (Benjamin & Scott 1979, Graham-Eagle 1983) and experimental results (Henderson & Miles 1994) parallel those discussed in this review. In some studies of Faraday wave experiments, the threshold acceleration depends strongly on the CL mobility (Nguyem-Thu-Lam & Caps 2011), whereas, in other studies, the presence of a CL has no effect on the modal structure. For example, Edwards & Fauve (1994) demonstrated the existence of pure Faraday waves in irregular-shaped containers. Perlin & Schultz (2000) suggested that improvements to CL models are necessary for additional progress in low-mode Faraday waves, which could explain why damping rates measured experimentally are much larger than the predictions. This comment parallels many of the results mentioned in this review in which CL motion dramatically influences the instability dynamics.

4. CONCLUDING REMARKS

Stability depends on the disturbance class. Going from volume to pressure disturbances destabilizes, whereas going from unpinned to pinned CL stabilizes. **Figure 10** summarizes this competition. The pressure disturbance with free CLs is the most dangerous, whereas the volume disturbance with pinned CLs is the least dangerous. These results hold for static and dynamic stability and, indeed, for any comparison for which disturbance classes are nested. For any particular capillary surface, the signature of this competition is nested stability windows, as illustrated in **Figure 7** for static bridges and **Figure 9*b*** for static rivulets.

The Steiner symmetrization construction extends the nesting idea. General disturbances are nested, in the sense of an energy ordering, within the rotationally symmetric disturbance class. Another tool, the Poincaré TP method, makes use of spectral ordering by parametric variation within a disturbance class. Disturbance classes often do not nest, and symmetry breaking often takes the system outside a disturbance class, in which case these tools are not available. In these cases, direct computation may be necessary.

The hydrodynamic stability of an inviscid disturbance is probed by normal modes $e^{i\lambda t}$. With the normal mode ansatz, the linear stability determination reduces to an eigenvalue problem

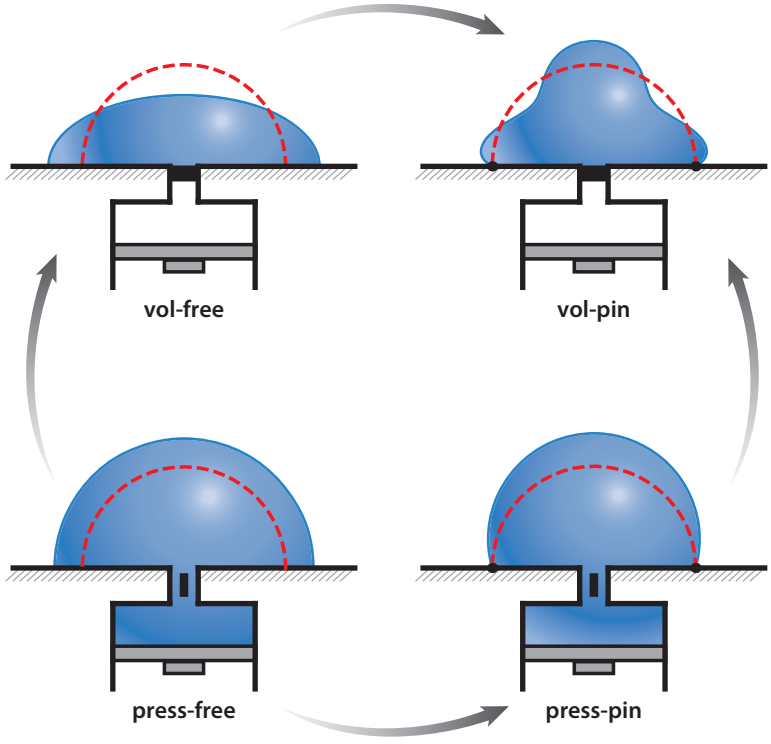

Figure 10

Schematic illustration of the relative stability to the pressure disturbances with free contact lines (press-free) and pinned contact lines (press-pin) and volume disturbances with free contact lines (vol-free) and pinned contact lines (vol-pin). Stabilization is in the direction of the arrows.

$\lambda^2 M\,[y] - K\,[y] = 0$ for the stationary shape disturbance y (Equation 18). Here M is a positive-definite operator representing the inertia (mass), and K is an indefinite operator representing the action of capillarity (spring constant). Constraints can be built into the operator or, alternatively, into the function space defining the disturbance class. Hydrodynamic instabilty is related to static instability through a negative eigenvalue of the self-adjoint eigenvalue problem $K\,[y] = \lambda y$ because a disturbance y yields static instability. A static disturbance y^* with negative eigenvalue λ^* of $\delta^2 F[y] \equiv K[y] = \lambda y$ corresponds to a growing dynamical disturbance because eigenvalue $\lambda^{**} = -ia\sqrt{-\lambda^*}$ with $a > 0$ by evaluating Equation 22 at y^*. For rotationally symmetric disturbances, this eigenvalue problem reduces to an ordinary differential equation, in which case Sturm comparison and separation theorems can be invoked to yield a priori results, as summarized in the spectral ordering and modal monotonicity sections (Sections 3.2.1 and 3.2.2).

We hope that the straightforward implications of the theory prove useful to the practitioner. For example, let us suppose the configurations in **Figure 2*a*,*d*,*g*** are in equilibrium (liquids and supports may differ). Surface curvatures can be scaled so that $k = \sin\alpha$ for all three, which yields $\chi = \cos\alpha - \bar{k}/\sin\alpha$. Then, because $\bar{k}_a < \bar{k}_d (= 0) < \bar{k}_g$ and in view of modal monotonicity, one can conclude that $\lambda_a < \lambda_d < \lambda_g$ for any eigenvalue solutions λ of the second variation (Equation 10). This means that configuration in **Figure 2*a*** is more stable than that in **Figure 2*d***, which is more stable than that in **Figure 2*g***. Moreover, for **Figure 2*d***, because $\chi_d = \cos\alpha$ and since λ_d is monotonic with χ, relative stabilization increases with wettability, a trend that also

holds for the sessile-drop frequencies. The ability of the CL to anchor, measured by χ, emerges as an important parameter for organizing families of results.

SUMMARY POINTS

1. For both static and dynamic problems and for all families, pinned-CL volume disturbances are the most stabilizing, whereas free-CL pressure disturbances are the least stabilizing.
2. For both the static and dynamic problems, tracking certain families of problems allows relative stability to be predicted a priori. Families following χ and the Noether mode are noteworthy.
3. For both static and dynamic self-adjoint problems with free CLs, eigenvalues increase with χ.
4. For the dynamic problem, the introduction of the lab frame, for example, to make the Rayleigh drop a sessile drop, breaks the translational invariance. This gives rise to walking instability (growth) and other low-frequency center-of-mass motions (oscillation), both inherited from the zero-frequency Noether mode.

FUTURE ISSUES

1. For CLs with mobility, Davis dissipation scales differently from viscous dissipation. Can these forms of dissipation be distinguished in experiment and in simulation? Can the walking instability be observed?
2. Spectral ordering for sessile drops can be broken for a range of wetting and spreading parameters. Can the metaphors of Schrödinger's equation and the periodic table be exploited for design purposes for drops as well as for liquid bridges and rivulets?
3. The Poincaré method builds on the isoperimetric problem in which there is a single constraint (volume). Many problems involve multiple constraints, as when a liquid bridge exerts a force at a variable length, along with a pressure at a variable volume. Can the Poincaré method be generalized to multiple constraints?
4. Steiner symmetrization applies to surfaces with a fixed wetted area (pinned CLs). Can one extend the symmetrization procedure to account for changes in the wetted area (moving CLs)?

DISCLOSURE STATEMENT

The authors are not aware of any biases that might be perceived as affecting the objectivity of this review.

ACKNOWLEDGMENTS

We thank A. Hirsa, M. Smith, D. Thiessen, H. van Lengerich, and C.T. Chang for supplying some of the experimental images and movies used in this review. P.H.S. thanks the NSF for support by grant CBET1236582.

LITERATURE CITED

Almeida ME, Teixeira HF, Koester LS. 2008. Preparation of submicron emulsions: theoretical aspects about the methods employed today. *Lat. Am. J. Pharm.* 27:780–88

Attinger D, Moore C, Donaldson A, Jafari A, Stone HA. 2013. Fluid dynamics topics in bloodstain pattern analysis: comparative review and research opportunities. *Forensic Sci. Int.* 231:375–96

Barz DPJ, Steen PH. 2013. A dynamic model of the electroosmotic droplet switch. *Phys. Fluids* 25:097104

Basaran OA. 2002. Small-scale free surface flows with breakup: drop formation and emerging applications. *AIChE J.* 48:1842–48

Basaran OA, DePaoli D. 1994. Nonlinear oscillations of pendant drops. *Phys. Fluids* 6:2923–43

Bauer H, Chiba M. 2004. Oscillations of captured spherical drop of frictionless liquid. *J. Sound Vib.* 274:725–46

Benilov E. 2009. On the stability of shallow rivulets. *J. Fluid Mech.* 636:455–74

Benilov E, Billingham J. 2011. Drops climbing uphill on an oscillating substrate. *J. Fluid Mech.* 674:93–119

Benjamin TB, Scott JC. 1979. Gravity-capillary waves with edge constraints. *J. Fluid Mech.* 92:241–67

Berthier E, Warrick J, Yu H, Beebe DJ. 2008. Managing evaporation for more robust microscale assays. Part 2. Characterization of convection and diffusion for cell biology. *Lab Chip* 8:860–64

Bigioni TP, Lin XM, Nguyen TT, Corwin EI, Witten TA, Jaeger HM. 2006. Kinetically driven self assembly of highly ordered nanoparticle monolayers. *Nat. Mater.* 5:265–70

Bisch C, Lasek A, Rodot H. 1982. Compartement hydrodynamique de volumes liquides spheriques semi-libres en apesanteur simulee. *J. Mec. Theor. Appl.* 1:165–84

Bolza O. 1904. *Lectures on the Calculus of Variations*. Chicago: Univ. Chicago Press

Borkar A, Tsamopoulos J. 1991. Boundary-layer analysis of the dynamics of axisymmetric capillary bridges. *Phys. Fluids A* 3:2866–74

Bostwick JB, Steen PH. 2009. Capillary oscillations of a constrained liquid drop. *Phys. Fluids* 21:032108

Bostwick JB, Steen PH. 2010. Stability of constrained cylindrical interfaces and the torus lift of Plateau-Rayleigh. *J. Fluid Mech.* 647:201–19

Bostwick JB, Steen PH. 2013a. Coupled oscillations of deformable spherical-cap droplets. Part 1. Inviscid motions. *J. Fluid Mech.* 714:312–35

Bostwick JB, Steen PH. 2013b. Coupled oscillations of deformable spherical-cap droplets. Part 2. Viscous motions. *J. Fluid Mech.* 714:336–60

Bostwick JB, Steen PH. 2014. Dynamics of sessile drops. Part 1. Inviscid theory. *J. Fluid Mech.* 760:5–38

Boudaoud A, Patricio P, Ben Amar M. 1999. The helicoid versus the catenoid: geometrically induced bifurcations. *Phys. Rev. Lett.* 83:3836–39

Boys C. 1959 (1890). *Soap Bubbles, Their Colours and the Forces Which Mold Them*. New York: Dover

Brakke KA. 1992. The surface evolver. *Exp. Math.* 1:141–65

Brown RA, Scriven LE. 1980a. On the multiple equilibrium shapes and stability of an interface pinned on a slot. *J. Colloid Interface Sci.* 78:528–42

Brown RA, Scriven LE. 1980b. The shape and stability of rotating liquid drops. *Proc. R. Soc. Lond. A* 371:331–57

Chandrasekhar S. 1987. *Ellipsoidal Figures of Equilibrium*. New York: Dover

Chang C, Bostwick JB, Steen PH, Daniel S. 2013. Substrate constraint modifies the Rayleigh spectrum of vibrating sessile drops. *Phys. Rev. E* 88:023015

Chen TY, Tsamopoulos J. 1993. Nonlinear dynamics of capillary bridges: theory. *J. Fluid Mech.* 255:373–409

Collicott SH, Weislogel MM. 2004. Computing existence and stability of capillary surfaces using surface evolver. *AIAA J.* 42:289–95

Courant R, Hilbert D. 1953. *Methods of Mathematical Physics*, Vol. I. New York: Wiley Intersci.

Culkin JB, Davis SH. 1983. Meandering of water rivulets. *AIChE J.* 30:263–67

Daniel S, Sircar S, Gliem J, Chaudhury M. 2004. Ratcheting motion of liquid drops on gradient surfaces. *Langmuir* 20:4085–92

Davis SH. 1980. Moving contact lines and rivulet instabilities. Part 1. The static rivulet. *J. Fluid Mech.* 98:225–42

de Gennes P. 1985. Wetting: statics and dynamics. *Rev. Mod. Phys.* 57:827–63

de Gennes P, Brochard-Wyart F, Quéré D. 2010. *Capillarity and Wetting Phenomena: Drops, Bubbles, Pearls, Waves*. New York: Springer

Introduces the mobility parameter and shows that the CL speed condition leads to an effective dissipation, even for inviscid fluids.

De Souza EJ, Gao L, McCarthy TJ, Arzt E, Crosby AJ. 2008. Effect of contact angle hysteresis on the measurement of capillary forces. *Langmuir* 24:1391–96
Delaunay C. 1841. Sur la surface de révolution dont la courbure moyenne est constante. *J. Math. Pure Appl.* 16:309–21
Dodds S, Carvalho MS, Kumar S. 2012. The dynamics of three-dimensional liquid bridges with pinned and moving contact lines. *J. Fluid Mech.* 707:521–40
Doedel EJ, Oldeman BE. 2009. AUTO-07P: continuation and bifurcation software for ordinary differential equations. **http://www.macs.hw.ac.uk/~gabriel/auto07/auto.html**
Dupré A. 1869. *Théorie Méchanique de La Chaleur*. Paris: Gauthier-Villars
Dussan V. E. 1979. On the spreading of liquids on solid surfaces: static and dynamic contact lines. *Annu. Rev. Fluid Mech.* 11:371–400
Dyson D. 1988. Contact line stability at edges: comments on Gibbs's inequalities. *Phys. Fluids* 31:229–32
Edwards WS, Fauve S. 1994. Patterns and quasi-patterns in the Faraday experiment. *J. Fluid Mech.* 278:123–48
Eggers J. 1997. Nonlinear dynamics and breakup of free-surface flows. *Rev. Mod. Phys.* 69:865–929
El-Genk MS, Saber HH. 2001. Minimum thickness of a flowing down liquid film on a vertical surface. *Int. J. Heat Mass Transf.* 44:2809–25
Erle M, Gillette R, Dyson D. 1970. Stability of interfaces of revolution with constant surface tension: the case of the catenoid. *Chem. Eng. J.* 1:97–109
Faraday M. 1831. On a peculiar class of acoustical figures, and on certain forms assumed by groups of particles upon vibrating elastic surfaces. *Philos. Trans. R. Soc. Lond.* 121:299–340
Fayzrakhmanova I, Straube A. 2009. Stick-slip dynamics of an oscillated sessile drop. *Phys. Fluids* 21:072104
Finn R. 1999. Capillary surface interfaces. *Not. AMS* 46:770–81
Gauss CF. 1830. *Principia generalia Theoriae Figurae Fluidorum in statu Aequilibrii*. Göttingen: Dieterichs
Gibbs JW. 1906. *The Scientific Papers of J. Willard Gibbs*, Vol. 1. London: Longmans, Green & Co.
Gillette R, Dyson D. 1971. Stability of fluid interfaces of revolution between equal solid circular plates. *Chem. Eng. J.* 2:44–54
Gillette R, Dyson D. 1972. Stability of axisymmetric liquid-fluid interfaces towards general disturbances. *Chem. Eng. J.* 3:196–99
Gillette R, Dyson D. 1974. Stability of static configurations with applications to the theory of capillarity. *Arch. Ration. Mech. Anal.* 53:150–77
Graham-Eagle J. 1983. A new method for calculating eigenvalues with applications to gravity-capillary waves with edge constraints. *Math. Proc. Camb. Philos. Soc.* 94:553–64
Grand-Piteira NL, Daerr A, Limat L. 2006. Meandering rivulets on a plane: a simple balance between inertia and capillarity. *Phys. Rev. Lett.* 96:254503
Harder PM, Shedd TA, Colburn M. 2008. Static and dynamic wetting characteristics of nano-patterned surfaces. *J. Adhes. Sci. Technol.* 22:1931–48
Henderson DM, Miles JW. 1994. Surface-wave damping in a circular cylinder with a fixed contact line. *J. Fluid Mech.* 275:285–99
Hirsa AH, López CA, Laytin M, Vogel MJ, Steen PH. 2005. Low-dissipation capillary switches at small scales. *Appl. Phys. Lett.* 86:014106
Hocking L. 1987. The damping of capillary-gravity waves at a rigid boundary. *J. Fluid Mech.* 179:253–66
Hormann G. 1887. *Untersuchung über die Grenzen, zwischen welchen Unduloide und Nodoide, die von zwei festen Parallelkreisflächen begrenzt sind, bei gegebenem Volumen ein Minimum der Oberfläche besitzen*. PhD Thesis, George-Augustus Univ., Göttingen
Howe W. 1887. *Die Rotationsflächen, welche bei vorgeschriebener Flächengröße ein möglichst großes oder kleines Volumen enthalten*. PhD Thesis, Friedrich-Wilhelms Univ., Berlin
Jain A, Toombes GE, Hall LM, Mahajan S, Garcia CB, et al. 2005. Direct access to bicontinuous skeletal inorganic plumber's nightmare networks from block copolymers. *Angew. Chem. Int. Ed. Engl.* 44:1226–29
Johns L, Narayanan R. 2002. *Interfacial Instability*. New York: Springer
Katz J. 1978. On the number of unstable modes of an equilibrium. *Mon. Not. R. Astron. Soc.* 183:765–70
Katz J. 1979. On the number of unstable modes of an equilibrium—II. *Mon. Not. R. Astron. Soc.* 189:817–22
Kidambi R. 2011. Frequency and damping of non-axisymmetric surface oscillations of a viscous cylindrical liquid bridge. *J. Fluid Mech.* 681:597–621

Kim H, Kim J, Kang B. 2004. Meandering instability of a rivulet. *J. Fluid Mech.* 498:245–56

Ko SH, Lee H, Kang KH. 2008. Hydrodynamic flows in electrowetting. *Langmuir* 24:1094–101

Kralchevsky PA, Denkov ND. 2001. Capillary forces and structuring in layers of colloid particles. *Curr. Opin. Colloid Interface Sci.* 6:383–401

Kumar S. 2015. Liquid transfer in printing processes: liquid bridges with moving contact lines. *Annu. Rev. Fluid Mech.* 47:67–94

Lafuma A, Quéré D. 2003. Superhydrophobic states. *Nat. Mater.* 2:457–60

Lamb H. 1932. *Hydrodynamics*. Cambridge, UK: Cambridge Univ. Press

Langbein D. 1990. The shape and stability of liquid menisci at solid edges. *J. Fluid Mech.* 213:251–65

Places the stability of capillary interfaces into the context of low-gravity experiments.

Langbein D. 2002. *Capillary Surfaces: Shape – Stability – Dynamics, in Particular Under Weightlessness*. Berlin: Springer-Verlag

Laplace R. 1806. *An Essay on the Cohesion of Fluids*. Paris: Coureier

Lappa M. 2005. Thermal convection and related instabilities in models of crystal growth from the melt on earth and in microgravity: past history and current status. *Cryst. Res. Technol.* 40:531–49

López CA, Lee C, Hirsa AH. 2005. Electrochemically activated adaptive liquid lens. *Appl. Phys. Lett.* 87:134102

Lowry B, Steen PH. 1995. Capillary surfaces: stability from families of equilibria with application to the liquid bridge. *Proc. R. Soc. Lond. A* 449:411–39

Lowry B, Steen PH. 1997. Stability of slender liquid bridges subjected to axial flows. *J. Fluid Mech.* 330:189–213

Lowry B, Thiessen D. 2007. Fixed contact line helical interfaces in zero gravity. *Phys. Fluids* 19:022102

Luzzatto-Fegiz P, Williamson CHK. 2012. Determining the stability of steady two-dimensional flows through imperfect velocity-impulse diagrams. *J. Fluid Mech.* 706:323–50

Lynden-Bell D, Wood R. 1968. The gravo-thermal catastrophe in isothermal spheres and the onset of red-giant structure for stellar systems. *Mon. Not. R. Astron. Soc.* 138:495–525

Lyubimov DV, Lyubimova TP, Shklyaev SV. 2004. Non-axisymmetric oscillations of a hemispheric drop. *Fluid Dyn.* 39:851–62

Lyubimov DV, Lyubimova TP, Shklyaev SV. 2006. Behavior of a drop on an oscillating solid plate. *Phys. Fluids* 18:012101

Develops TP theorems for isoperimetric problems that are related to pressure and volume disturbances for capillary surfaces.

Maddocks JH. 1987. Stability and folds. *Arch. Ration. Mech. Anal.* 99:301–28

Maddocks JH, Sachs RL. 1995. Constrained variational principles and stability in Hamiltonian systems. In *Hamiltonian Dynamical Systems*, ed. H Dumas, K Meyer, D Schmidt, pp. 231–64. New York: Springer

Malouin B, Vogel MJ, Hirsa AH. 2010. Electromagnetic control of coupled droplets. *Appl. Phys. Lett.* 96:214104

Mampallil D, van den Ende D, Mugele F. 2011. Controlling flow patterns in oscillating sessile drops by breaking azimuthal symmetry. *Appl. Phys. Lett.* 99:154102

Matar O, Craster R. 2009. Dynamics of surfactant-assisted spreading. *Soft Matter* 5:3801–9

Matsumoto T, Nogi K. 2008. Wetting in soldering and microelectronics. *Annu. Rev. Mater. Res.* 38:251–73

Maugis D. 2000. *Contact, Adhesion and Rupture of Elastic Solids*. New York: Springer

Maxwell J. 1898. *Encyclopedia Britannica*. Edinburgh: Adam & Charles Black. 9th ed.

May H, Lowry B. 2008. Microgravity/microscale double-helical fluid containment. *Proc. R. Soc. A* 464:855–75

McKinley GH, Sridhar T. 2002. Filament-stretching rheometry of complex fluids. *Annu. Rev. Fluid Mech.* 34:375–415

Michael D. 1981. Meniscus stability. *Annu. Rev. Fluid Mech.* 13:189–215

Sets forth the mathematical approach to the stability of capillary surfaces, motivated by the low-gravity application and with a large number of references.

Miles J, Henderson D. 1990. Parametrically forced surface waves. *Annu. Rev. Fluid Mech.* 22:143–65

Milne A, Defez B, Cabrerizo-Vílchez M, Amirfazli A. 2014. Understanding (sessile/constrained) bubble and drop oscillations. *Adv. Colloid Interface Sci.* 203:22–36

Mollot D, Tsamopoulos J, Chen T, Ashgriz N. 1993. Nonlinear dynamics of capillary bridges: experiments. *J. Fluid Mech.* 255:411–35

Muralidharan S, Voorhees PW, Davis SH. 2013. Nonaxisymmetric droplet unpinning in vapor-liquid-solid-grown nanowires. *J. Appl. Phys.* 114:114305

Myshkis A, Babskii V, Slobozhanin N, Tyuptsov A. 1987. *Low-Gravity Fluid Mechanics*. New York: Springer

Nakagawa T, Nakagawa R. 1996. A novel oscillation phenomenon of the water rivulet on a smooth hydrophobic surface. *Acta Mech.* 115:27–37

Nakagawa T, Scott J. 1992. Rivulet meanders on a smooth hydrophobic surface. *Int. J. Multiphase Flow* 18:455–63
Nguyem-Thu-Lam K, Caps H. 2011. Effect of a capillary meniscus on the Faraday instability threshold. *Eur. Phys. J. E* 34:112
Noblin X, Buguin A, Brochard-Wyart F. 2004. Vibrated sessile drops: transition between pinned and mobile contact lines. *Eur. Phys. J. E* 14:395–404
Noblin X, Buguin A, Brochard-Wyart F. 2005. Triplon modes of puddles. *Phys. Rev. Lett.* 94:166102
Noblin X, Kofman R, Celestini F. 2009. Ratchet-like motion of a shaken drop. *Phys. Rev. Lett.* 19:194504
Oh JM, Ko SH, Kang KH. 2008. Shape oscillation of a drop in ac electrowetting. *Langmuir* 24:8379–86
Oron A, Davis SH, Bankoff SG. 1997. Long-scale evolution of thin liquid films. *Rev. Mod. Phys.* 69:931–80
Paulsen JD, Burton JC, Nagel SR, Appathurai S, Harris MT, Basaran OA. 2012. The inexorable resistance of inertia determines the initial regime of drop coalescence. *Proc. Natl. Acad. Sci. USA* 109:6857–61
Perlin M, Schultz WW. 2000. Capillary effects on surface waves. *Annu. Rev. Fluid Mech.* 32:241–74
Plateau J. 1863. Experimental and theoretical researches on the figures on equilibrium of a liquid mass withdrawn from the action of gravity, etc. In *Annual Report of the Board of Regents of the Smithsonian Institution*, pp. 207–85. Washington, DC: Smithsonian Inst.
Poincaré H. 1885. Sur l'équilibre d'une masse fluide animée d'un mouvement de rotation. *Acta Math.* 7:259–380
Prosperetti A. 2012. Linear oscillations of constrained drops, bubbles, and plane liquid surfaces. *Phys. Fluids* 24:032109
Quéré D. 1999. Fluid coating on a fiber. *Annu. Rev. Fluid Mech.* 31:347–84
Ramalingam SK, Basaran OA. 2010. Axisymmetric oscillation modes of a double droplet system. *Phys. Fluids* 22:112111
Ramalingam SK, Ramkrishna D, Basaran OA. 2012. Free vibrations of a spherical drop constrained at an azimuth. *Phys. Fluids* 24:082102
Rayleigh L. 1879. On the capillary phenomenon of jets. *Proc. R. Soc. Lond.* 29:71–97
Rowlinson J, Widom B. 2002. *Molecular Theory of Capillarity*. New York: Dover
Roy R, Schwartz L. 1999. On the stability of liquid ridges. *J. Fluid Mech.* 391:293–318
Rücker AW. 1886. On the critical mean curvature of liquid surfaces of revolution. *Philos. Mag.* 23:35–45
Russo MJ, Steen PH. 1986. Instability of rotund capillary bridges to general disturbances: experiment and theory. *J. Colloid Interface Sci.* 113:154–63
Sambath K, Basaran OA. 2014. Electrohydrostatics of capillary switches. *AIChE J.* 60:1451–59
Sariola V, Jääskeläinen M, Zhou Q. 2010. Hybrid microassembly combining robotics and water droplet self-alignment. *IEEE Trans. Robot.* 26:965–77
Schmuki P, Laso M. 1990. On the stability of rivulet flow. *J. Fluid Mech.* 215:125–43
Schrödinger E. 1915. Notiz über den kapillardruck in gasblasen. *Ann. Phys.* 46:1413–18
Seetharaman S, Teng L, Hayashi M, Wang L. 2013. Understanding the properties of slags. *ISIJ Int.* 53:1–8
Segner J. 1751. De figuris superficierum fluidarum. *Soc. Reg. Goetting.* 1:301–72
Shahraz A, Borhan A, Fichthorn KA. 2012. A theory for the morphological dependence of wetting on a physically patterned solid surface. *Langmuir* 28:14227–37
Sharp J. 2012. Resonant properties of sessile droplets: contact angle dependence of the resonant frequency and width in glycerol/water mixtures. *Soft Matter* 8:399–407
Sharp J, Farmer D, Kelly J. 2011. Contact angle dependence of the resonant frequency of sessile water droplets. *Langmuir* 27:9367–71
Shikhmurzaev YD. 2007. *Capillary Flows with Forming Interfaces*. Boca Raton, FL: Chapman & Hall/CRC
Slater DM, Vogel MJ, Macner AM, Steen PH. 2012. Beetle-inspired adhesion by capillary-bridge arrays: pull-off detachment. *J. Adhes. Sci. Technol.* 28:273–89
Slobozhanin LA, Alexander JID. 2003. Stability diagrams for disconnected capillary surfaces. *Phys. Fluids* 15:3532–45
Slobozhanin LA, Alexander JID, Resnick AH. 1997. Bifurcation of the equilibrium states of a weightless liquid bridge. *Phys. Fluids* 9:1893–905

Slobozhanin LA, Shevtsova VM, Alexander JID, Meseguer J, Montanero JM. 2012. Stability of liquid bridges between coaxial equidimensional disks to axisymmetric finite perturbations: a review. *Microgravity Sci. Technol.* 24:65–77

Snoeijer JH, Andreotti B. 2013. Moving contact lines: scales, regimes, and dynamical transitions. *Annu. Rev. Fluid Mech.* 45:269–92

Steiner J. 1882. *Gesammelte Werke*. Berlin: Reimer

Shows that the introduction of a spherical-bowl constraint introduces a new low-frequency mode not present for free drops.

Strani M, Sabetta F. 1984. Free vibrations of a drop in partial contact with a solid support. *J. Fluid Mech.* 141:233–47

Sui Y, Ding H, Spelt PD. 2014. Numerical simulations of flows with moving contact lines. *Annu. Rev. Fluid Mech.* 46:97–119

Theisen EA, Vogel MJ, López CA, Hirsa AH, Steen PH. 2007. Capillary dynamics of coupled spherical-cap droplets. *J. Fluid Mech.* 580:495–505

Thiessen DB, Marr-Lyon MJ, Marston PL. 2002. Active electrostatic stabilization of liquid bridges in low gravity. *J. Fluid Mech.* 457:285–94

Thomas EL, Anderson DM, Henkee CS, Hoffman D. 1988. Periodic area-minimizing surfaces in block copolymers. *Nature* 334:598–601

Thompson J. 1979. Stability predictions through a succession of folds. *Philos. Trans. R. Soc. Lond. A* 292:1–23

Tsamopoulos J, Chen TY, Borkar A. 1992. Viscous oscillations of capillary bridges. *J. Fluid Mech.* 235:579–609

Tuteja A, Choi W, Ma M, Mabry JM, Mazzella SA, et al. 2007. Designing superoleophobic surfaces. *Science* 318:1618–22

van Lengerich HB, Steen PH. 2012. Energy dissipation and the contact-line region of a spreading bridge. *J. Fluid Mech.* 703:111–41

van Lengerich HB, Vogel MJ, Steen PH. 2010. Coarsening of capillary drops coupled by conduit networks. *Phys. Rev. E* 82:066312

Vejrazka J, Vobecka L, Tihon J. 2013. Linear oscillations of a supported bubble or drop. *Phys. Fluids* 25:062102

Vogel MJ, Ehrhard P, Steen PH. 2005. The electroosmotic droplet switch: countering capillarity with electrokinetics. *Proc. Natl. Acad. Sci. USA* 102:11974–79

Vogel MJ, Steen PH. 2010. Capillarity-based switchable adhesion. *Proc. Natl. Acad. Sci. USA* 107:3377–81

Vukasinovic B, Smith M, Glezer A. 2007. Dynamics of a sessile drop in forced vibration. *J. Fluid Mech.* 587:395–423

Weiland RH, Davis SH. 1981. Moving contact lines and rivulet instabilities. Part 2. Long waves on flat rivulets. *J. Fluid Mech.* 107:261–80

Wente HC. 1999. A surprising bubble catastrophe. *Pac. J. Math.* 189:339–75

Xu XM, Vereecke G, van den Hoogen E, Smeers J, Armini S, et al. 2013. Wetting challenges in cleaning of high aspect ratio nano-structures. *Solid State Phenom.* 195:235–38

Young GW, Davis SH. 1987. Rivulet instabilities. *J. Fluid Mech.* 176:1–31

Young T. 1805. An essay on the cohesion of fluids. *Philos. Trans. R. Soc. Lond.* 95:65–87

RELATED RESOURCES

Bernate JA, Thiessen DB. 2012. Stability of capillary surfaces supported by a helical wire. APS DFD Gallery Fluid Motion video. **http://arxiv.org/abs/1210.4100**. Illustrates stabilizing liquid columns by helical supports.

Chang C-T, Daniel S, Steen PH. 2013. Excited sessile drops dance harmonically. YouTube video. **http://www.youtube.com/watch?v=Bk7xh4DqkiY**. Shows a classification scheme for the identification of mechanically oscillated sessile drops.

Annual Review of
Fluid Mechanics

Volume 47, 2015

Contents

Indexes

Errata

An online log of corrections to *Annual Review of Fluid Mechanics* articles may be found at http://www.annualreviews.org/errata/fluid